Accepted Manuscript

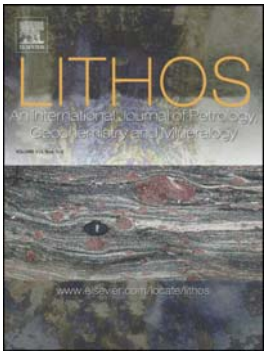

Diamonds from Dachine, French Guiana: a unique record of Early Proterozoic subduction

Chris B. Smith, Michael J. Walter, Galina P. Bulanova, Sami Mikhail, Antony D. Burnham, Luiz Gobbo, Simon C. Kohn

PII: S0024-4937(16)30315-2
DOI: doi: 10.1016/j.lithos.2016.09.026
Reference: LITHOS 4087

To appear in: *LITHOS*

Received date: 14 April 2016
Revised date: 7 September 2016
Accepted date: 17 September 2016

Please cite this article as: Smith, Chris B., Walter, Michael J., Bulanova, Galina P., Mikhail, Sami, Burnham, Antony D., Gobbo, Luiz, Kohn, Simon C., Diamonds from Dachine, French Guiana: a unique record of Early Proterozoic subduction, *LITHOS* (2016), doi: 10.1016/j.lithos.2016.09.026

Diamonds from Dachine, French Guiana: a unique record of Early Proterozoic subduction

Chris B. Smith[a], Michael J. Walter[a], Galina P. Bulanova,[a], Sami Mikhail[a,b], Antony D. Burnham[a,c], Luiz Gobbo[d], and Simon C. Kohn[a]

[a]School of Earth Sciences, University of Bristol, Queen's Road, Bristol, United Kingdom

[b]Department of Earth and Environmental Sciences, The University of St. Andrews, St. Andrews, United Kingdom

[c]Research School of Earth Sciences, Australian National University, Canberra, Australia.

[d]Rio Tinto Desinvolvimentos Minerais Ltd., Brasilia, Brazil.

Corresponding author: M.J. Walter (m.j.walter@bristol.ac.uk)

Abstract

Diamonds from Dachine, French Guiana, are unique among worldwide diamond populations. The diamonds were transported to the surface in an unusual ultramafic extrusive magma with an affinity to boninite or komatiite, which was emplaced within an arc geological setting at ~ 2.2 Ga. Dachine diamonds have internal and external morphologies indicative of relatively rapid growth from carbon oversaturated fluids or melts, and exhibit internal features consistent with residence in a high-strain environment. On the basis of nitrogen (N) defects the diamonds are categorized as Type Ib-IaA. The unusually low aggregation state of N places severe constraints on the thermal history of the diamonds, effectively ruling out derivation in convecting mantle. The carbon and N isotopic compositions of Dachine diamonds are consistent with a sedimentary source of carbon, with the majority of diamonds having $\delta^{13}C$ values < -25‰ and $\delta^{15}N$ values > +4‰. The primary carbon was presumably deposited on an early Proterozoic seafloor. Sulphide inclusions have low Ni and Cr and are comparable to lithospheric eclogitic-type sulphide inclusions. Three garnet and one clinopyroxene inclusion are also eclogitic in composition, and one garnet inclusion has a majorite

component indicating an origin around 250 km depth. The silicate inclusions are highly depleted in many incompatible trace elements (e.g. LREE, Nb, Hf, Zr), and modelling indicates an eclogitic source lithology that contained a LREE-enriched trace phase such as epidote or allanite, and an HFSE-rich phase such as rutile. Four of the five inclusions are unusually enriched in Mn, as well as Ni and Co, and modelling indicates a protolith with the bulk composition of subducted normal MORB plus about 10% ferromanganese crust component. We suggest a model wherein Dachine diamonds precipitated from remobilized sedimentary carbon at the slab-mantle interface from liquids derived ultimately by deserpentinization of slab peridotite at depths of ~ 200 to 250 km. These fluids may also trigger melting in wedge peridotite, resulting in a volatile-rich ultramafic melt that transports the diamonds rapidly to the surface. The process of diamond formation and exhumation from the slab mantle interface likely occurred in a Paleoproterozoic subduction zone and over a very limited timespan, likely less than a million years.

Keywords: Dachine, Diamond, Inclusions, Subduction, Isotopes

1. Introduction

The vast majority of natural diamonds form at high pressures in mantle rocks, sampling a carbon-rich source at depth (Shirey et al., 2013), and there is strong evidence that diamonds crystallize as products of fluid or melt metasomatism (Klein-BenDavid et al., 2010; Navon et al., 1988; Walter et al., 2008). Diamonds are nearly pure carbon, but incorporate chemical defects, the most prominent of which is N (Taylor et al., 1990). Diamonds also record local chemical equilibria by entrapping phases as they grow, including minerals, fluids and melts. Because of their great physical resilience, diamonds can preserve these internal features in pristine form over geological time-scales, features that reveal important information about the petrologic, tectonic and geodynamic environment in which they grew, e.g. (Bulanova et al., 2010; Cartigny, 2005; Gurney et al., 2010; Haggerty, 1999; Pearson and Wittig, 2008; Shirey et al., 2013; Shirey et al., 2002; Stachel and Harris, 2008; and Harris, 2009; Walter et al., 2011).

Most diamonds sampled at the surface originated in ancient cratonic lithosphere, and their mode of genesis has provided unique insights into how cratons form and evolve (Cartigny et al., 1998; Gurney et al., 2010; Pearson and Wittig, 2008; Shirey et al., 2013; Shirey et al., 2002; Stachel and Harris, 2008). Other much rarer diamonds contain inclusions that place their origin in sub-lithospheric mantle, some as deep as the lower mantle, and many of these so-called ‘superdeep’ diamonds show evidence for an origin related to subduction of carbon-rich lithologies into the deep convecting mantle (Brenker et al., 2007; Harte, 2010; Harte et al., 1999; Stachel et al., 2005; Walter et al., 2011). Here we report on a unique suite of diamonds from Dachine, French Guiana, which in many ways are unlike their lithospheric or superdeep cousins, and for which a definitive origin has proven elusive.

To begin, Dachine diamonds are unusual in that they are found in a Paleoproterozoic host rock that has been described as a metamorphosed pyroclastic ultramafic extrusive, with chemical features indicative of a komatiite (Bailey, 1999; Capdevila et al., 1999; Magee and Taylor, 1999). Capdevila

et al. suggest a depth of origin > 250 km for Dachine diamonds on the basis of the inferred depth at which a putative komatiitic host magma would be generated. Cartigny (2010) related Dachine diamonds to carbonado on the basis of their similar isotopic compositions, and suggested they originate in the mantle at depths > 300 km, crystallizing from volatiles components associated with komatiite formation. Previous conclusions about the origins of Dachine diamonds were made in the absence of any silicate inclusions that could place limits on the depth of formation and lithologies involved.

Here we present a comprehensive study of Dachine diamonds and, for the first time, report on sulphide and silicate mineral inclusions. We provide new textural, chemical and isotopic data from the diamonds, and crystal chemical data from mineral inclusions, and use this information to interpret the petrologic and geodynamic history of diamond growth. We conclude that the diamonds originated in a subduction zone environment in the region of the slab-mantle interface at depths around ~ 200 to 250 km, and from carbon derived originally on the seafloor. We further deduce that the diamonds had only a short residence time in the mantle before being sampled by a unique, volatile-rich magma formed in a subduction setting.

1.1. Geological context

The Dachine ultramafic body is located in an arc-type setting and forms part of the Transamazonian Lower Paramaca greenstone orogenic belt in southern French Guiana (Bailey, 1999; Capdevila et al., 1999). The Paramaca series, dated at ~ 2.11 Ga to 2.25 Ga (Gruau et al., 1985; Tassinari et al., 1989), consists mainly of metabasalts and overlying felsic gneisses derived from volcanic sediments, dacitic and rhyolitic tuffs, and lavas. The Dachine ultramafic unit has been metamorphosed to talc schist, with preserved volcaniclastic textures indicative of a pyroclastic deposit (Bailey, 1999). The ultramafic has been described as a komatiite based on its major and trace element chemistry (Bailey, 1999; Capdevila et al., 1999), although its exact pedigree remains uncertain. Magee et al. (1999) and Magee (2001) show that chromite compositions from Dachine

are distinct from komatiitic chromites, and suggest the source rock was a picritic shoshonite. Wyman et al. (2008), based on a comparison with the properties of diamondiferous lamprophyres in Canada, suggested the host rock may be an adakitic lamprophyre similar to those hosting diamonds in late-Archean (2.7 Ga) deposits at Wawa in Quebec (Wyman et al., 2006). What is clear is that the Dachine unit is unusual because it is diamond-bearing, but it is not a kimberlite or lamproite within which most diamonds are typically found.

Figure 1 is a trace element compatibility diagram showing a compilation of whole rock incompatible trace element data for the Dachine host rock, compared to mean compositions of a variety of mafic and ultramafic rock types, all normalised to primitive mantle. The Dachine ultramafic is generally more depleted than MORB, except in the more incompatible elements. It is similar in character to komatiite, perhaps even more so to boninite, and is also similar to the Wawa adakitic lamprophyre; it is clearly not akin to kimberlite. On the basis of the arc tectonic setting of the Paramaca greenstone belt together with its pyroclastic character and the geochemical affinities exhibited in figure 1, we suggest that the Dachine host rock was derived in a subduction zone setting, likely involving a volatile-rich source.

2. Materials and Methods

2.1 Samples

Forty-eight inclusion-bearing diamonds were selected for polishing and comprehensive study from a suite of one hundred and thirty diamonds recovered from bulk samples and drill core during prospecting operations on the Dachine ultramafic body. Diamonds were examined optically under a binocular microscope, photographed, and their morphology and surface features described and classified. Central diamond plates parallel to the dodecahedral plane were prepared by polishing on a diamond wheel at the University of Bristol. Mineral inclusions were also exposed for analysis by polishing.

2.2 Analytical methods

2.2.1 Optical properties of diamonds

Long wavelength ultraviolet light was used to categorise diamond fluorescence using a Leningrad Optical Mechanical Enterprise instrument OE-18A. The light source was a Hg quartz lamp fitted with a 265 nm wavelength filter. Cathodoluminescence images were taken with a JSM-35 scanning electron microscope (I=3 nA, V=20 kV) at the University of Bristol. These images were used to define the nature of internal crystal growth.

2.2.2 FTIR for defect characterisation of diamonds

Fourier transform infrared (FTIR) spectra of double-polished diamond plates were recorded using a Nicolet iN10MX infrared microscope over the range 675 – 4000 cm^{-1}. Following manual baseline subtraction, the spectra obtained were normalised to an absorbance of 12.3 at 2000 cm-^{1} (Hardy and Smith, 1961). Spectral deconvolution was performed using the spreadsheet caxbd97n.xls (D. Fisher, pers. comm.).

2.2.3 Carbon and nitrogen isotopes

Off-cuts from diamond plate preparation weighing between 0.12 to 0.94 mg were analysed by stepped-combustion. The $\delta^{13}C$-, $\delta^{15}N$-values and N concentrations were obtained simultaneously on samples treated by a single temperature programme using three fully automated static-mode mass spectrometers fed from a common extraction system under high vacuum at the Open University, U.K. The $\delta^{13}C$, $\delta^{15}N$ and N/C ratio data were obtained according to the methods outlined in Mikhail et al. (2014) and the values reported here are weighted mean values for each fragment analysed. The blank levels for N in the system averaged 0.5 ± 0.2 ng of N per combustion step above 700 °C (n = 79). N concentrations were measured in ppm with an accuracy of better than 10%. $\delta^{13}C$ and $\delta^{15}N$ stable isotopic compositions are expressed relative to PDB (for C) and air (for N) standards in parts per mil (‰) with an average analytical precision better than ± 0.6 ‰ (2σ). The accuracy of

$\delta^{15}N$ is inclusive of the blank correction and is therefore larger than the precision using international and in house standard materials (Mikhail et al., 2014).

2.2.4 Electron microprobe analyses

Major and minor element compositions of exposed and polished mineral inclusions were measured using electron microprobe analysis the University of Bristol with a Cameca SX100, and with a beam current of 20 nA at 15 kV voltage, and a spot size of ~1 micron at the surface. Silicate and oxide standards and conventional PAP data reduction techniques were employed, and replicate analysis of standards yields uncertainties at the 2 and 5% level, respectively, for major and minor elements.

2.2.5 Secondary ion mass spectrometry

Trace element concentrations in silicate inclusions were determined using a Cameca IMS-4f ion-microprobe at the Edinburgh Ion Microprobe Facility. Samples were cleaned and pressed into indium mounts and gold-coated for analyses. The primary beam of $^{16}O^-$ ions was ~11 keV (~15 keV net impact energy), with a sample current of 2 nA, which corresponds to a spatial resolution of ~15 μm at the sample surface. The secondary ion accelerating voltage of 4,500 V was offset by 75 eV (energy window of 40 eV) to reduce molecular ion transmission. Analyses were made in two consecutive passes measuring the 'light' and 'heavy' elements respectively. In each pass five sweeps of the desired masses were made, and the spectrometer position for each element was adjusted manually during the first sweep. Multiple elements were analysed in both passes to ensure internally consistency. Raw data were reduced using custom in-house software.

Calibration was performed on glass standards under identical operating conditions, The silicate glass standard srm610 was used, as in previous studies (Bulanova et al., 2010; Walter et al., 2008). Statistical precision at concentrations >1 ppm is better than 10% relative for all isotopes. Accuracy is better than 10% relative for the rare-earth elements (REE), Ba, Sr, Nb, Zr and Y, and is within

30% relative for Hf, Rb, Th and U (R. Hinton, personal communication). Background levels were determined by counting on mass 130.5, and all analyses falling below these levels were excluded.

3. Data and Observations

3.1 Diamond Morphology and Internal Structure

Dachine diamonds are small (1 mm or less), with 71% having step-layered octahedral external form with a polycentric internal growth structure. Minor cubo-octahedra are present (15%), cubes are rare and aggregates are absent. Many diamonds show natural breakages, but resorption is minimal. In colour they range from pale greyish yellow to pale brown. External morphologies of alluvial and eluvial stones nearby to Dachine (McCandless et al., 1999) are consistent with our observations.

Cathodoluminescent imaging (CL) of polished central diamond plates reveals complex structures, examples of which are shown in figure 2. Internally the diamonds either show blocky, sectorial, granular growth structures or have octahedral zonation and intensive plastic deformation (Fig 2a, b, d). The thin diamond rims display regular octahedral growth (Fig. 2a). Fibrous growth was found only in the rim of one cubo-octahedral/aggregate diamond (Fig. 2c). Etch channels and cracks are common at the crystal margins, exploiting boundaries of internal blocks (Fig. 2b). Twenty one stones were examined under long wavelength ultraviolet light, with eight showing no apparent luminescence, eight others exhibiting a combination of pale yellowish green with pale blue patches, three pale blue, and two showing pale pink fluorescence.

3.2 Nitrogen Content and Defects

Representative FTIR spectra are shown in figure 3. Seven out of nineteen samples have spectra containing N-related features that can be fitted with components for C (single neutral N defects), A (paired neutral N defects) and X (N+ defects, Lawson et al., 1998). The coexistence of C and A defects means that most of the diamonds are classified as type Ib-IaA. Diamonds with no detectable N defects are classified as type II. Some spectra contain a feature between the A and C peaks that

could be attributed to the Y-centre, a defect of uncertain origin (Hainschwang et al., 2012). Modifying the fitting procedure to account for this extra component resulted in minimal changes to the calculated N content and aggregation state, and therefore it is not considered further. Of the remaining twelve samples, seven showed spectral features reminiscent of the F-defect (Hainschwang et al., 2012; Woods and Collins, 1983).

In spectra of many of the type Ib and IIa diamonds there were low intensity narrow peaks (half width at half maximum ~1.7 cm^{-1} at the resolution used) at 1353, 1359, 1374, 1405, 3107, 3144 and 3182 cm^{-1}, many of which have been attributed to the presence of H or interstitials/vacancies (Fisher and Lawson, 1998; Fritsch et al., 2007); these defects did not generally correlate in intensity. Some diamonds had no detectable N (less than about 5 ppm with our equipment and procedures, but varying somewhat, depending on sample thickness, the presence or absence of inclusions, etc), but these samples are not recorded in figure 3. The mean N concentration is hence lower than implied by the choice of data shown in the figure. With the exception of the complexities mentioned above, the range of N concentration and aggregation is similar that reported by Cartigny (2010) and the results for N concentration by FTIR and mass spectrometry (Table 1) for diamonds in our sample suite are also consistent. The key finding from FTIR is that the Dachine diamonds have very low N aggregation compared with the worldwide diamond populations where >99% do not show single N defects (Allen and Evans, 1981), placing strong constraints on the thermal history of the diamonds between their growth and exhumation.

3.3 Carbon and Nitrogen Isotope Values

Carbon and nitrogen data for Dachine diamonds are provided in Table 1, and isotopic compositions are plotted in figure 4. The results show ranges for $\delta^{15}N$ and $\delta^{13}C$ of -5 to +21 ‰ and 0 to -36 ‰, respectively, with a mean N concentration of 20 ppm. Such ^{13}C-depletion relative to the mantle values and the low N concentrations with a high proportion of Type II diamonds are consistent with prior observations of Dachine diamonds (Cartigny, 2010; McCandless et al., 1999). The identified

^{15}N-enrichment for the Type II samples (this study) are similar to Type I samples (Cartigny, 2010), and we observed no statistically significant rerlationships among $\delta^{13}C$, $\delta^{15}N$, and N concentration. Overall, the data show that Dachine diamonds are characterised by extremely negative $\delta^{13}C$ and positive $\delta^{15}N$ values compared to typical eclogitic and peridotitic populations of lithospheric diamonds, and have stable isotope values more akin to diamondites and carbonado.

3.4 Mineral Inclusions

We exposed silicate (garnet and clinopyroxene) and sulphide mineral inclusions in twenty three Dachine diamonds. The syngenetic nature of these inclusions is indicated by an absence of associated cracks to the surface, and octahedral morphology imposed on the inclusions by the diamond-host (Bulanova et al., 2005; Meyer, 1987). Sulfide is the most common inclusion and grains were analysed from eighteen diamonds. Spessartine-rich garnet was found in three separate diamonds, and two other diamonds contained clinopyroxene. We note that no single diamond contained both garnet and clinopyroxene. A single inclusion of SiO_2 was exposed in one Dachine diamond. Epigenetic minerals in two diamonds, identified on the basis of cracks in the diamonds that extend to the surface, consist of fluorite and an unresolved Na-Al-Cr-Fe silicate.

3.4.1 Garnet

Major and minor element compositions of silicate inclusions are given in Table 2, and trace element data in Table 3. Garnet inclusions from three diamonds have an unusually high spessartine content, with the three garnet grains having MnO contents ranging from 13 to 19 wt%, as shown in figure 5. The garnet inclusions are also pyrope-rich, and can be classified as eclogitic in composition on the basis of their high-Ca and extremely low-Cr abundances. Figure 5 shows that their high spessartine component resembles garnet from skarn haloes around sulphide ore-bodies of Broken Hill type (e.g. Balfour Copper Belt, Tasmania), garnet associated with volcanogenic massive sulphide (VMS) deposits such as at Abitibi, Canada and Pecos, New Mexico, and garnet from gondite associations such as those in northern Ghana. However, the pyrope component in Dachine garnet inclusions is

considerably higher than in other high-Mn garnet from any of these locations, consistent with an origin in a mafic protolith. The garnet inclusion compositions are also quite distinct from garnet in Dachine drill core concentrates (Bailey, 1999), which have predominately crustal almandine compositions with low MnO values (Fig 5). A small number of mantle-derived peridotitic pyrope garnet minerals were reported in host rock concentrates by Bailey (1999), including some weakly depleted harzburgitic garnet, but none were observed as silicate inclusions in our study. Possible eclogitic garnet with little or no Na are also present in the concentrates, but none of these show Mn-enrichment. To our knowledge, the Dachine garnet inclusion major element compositions are unique, and have not been reported from inclusions in diamonds or mantle xenoliths elsewhere.

The trace element compositions of Dachine garnet inclusions are shown in figure 6. The garnets are characteristically depleted in large ion lithophile elements (LILE) and light rare earth elements (LREE) relative to primitive mantle. Overall the REE are highly fractionated, with the LREE depleted and the HREE enriched relative to primitive mantle. Two of the three garnets show a minor negative Eu anomaly, consistent with a subducted oceanic crustal protolith. Figure 6 also shows La versus Yb for the garnet inclusions relative to lithospheric and sublithospheric garnet inclusions in diamonds as well as inclusions in diamondites. The Dachine inclusions have compositions lying at the extreme high Yb end of the spectrum of all inclusions, and are relatively depleted in La. They are closest in composition to the most depleted eclogitic lithospheric and diamondite garnet inclusions. High field strength elements (HFSE) like Nb, Zr and Hf also lie at the more depleted end of the spectrum defined by garnet inclusions in diamond (not shown). Although we have limited samples, it would seem that not only do the Dachine garnet inclusions have unusually high Mn-contents, their trace element contents are atypical of most garnet inclusions in diamonds.

3.4.2 Clinopyroxene

The two clinopyroxene inclusion compositions are plotted in the pyroxene ternary in figure 7. Neither inclusion falls in the field occupied by peridotitic clinopyroxene inclusions in lithospheric diamonds, but instead are akin to eclogitic clinopyroxene inclusions. One of the pyroxene inclusions is Mn-rich (4.6% MnO, Table 2), the other is Mn poor. The Mn-poor inclusion has a relatively high jadeite component (~27%), and an overall composition that is typical of eclogitic clinopyroxene. In contrast, the Mn-rich pyroxene has a small jadeite component (~ 4%), and falls outside the range of normal eclogitic pyroxene. Given the unusually Mn-rich composition we will not attempt to classify this pyroxene further, except to say that it is mafic rather than peridotitic.

The trace element compositions of the clinopyroxenes are shown in figure 8. The inclusions are depleted in incompatible elements overall, and have about an order of magnitude lower LREE than world-wide clinopyroxene inclusions in diamond. Their La contents are the most depleted among lithospheric eclogitic clinopyroxene inclusions (Fig. 8 inset), and Gd/Lu is low in one inclusion. The clinopyroxene inclusion with low Mn is conspicuously depleted in HREE. Thus, like the garnet inclusions, Dachine clinopyroxene inclusions have a mafic major element character, but show unique depletions in incompatible lithophile elements.

3.4.3 Garnet – clinopyroxene thermobarometry

The compositions of the garnet and clinopyroxene inclusions can yield estimates of pressure and temperature of origin. One of the three garnet inclusions has a notable silica excess in the structural formula of ~0.07, and applying the majorite garnet barometer of Collerson et al. (2010) yields a pressure of ~ 7.7 ±0.5 GPa, which would place inclusion formation at about 250 km depth. The remaining two garnets do not have excess silica, and must have formed shallower. Although the silicate inclusions all occur in separate diamonds, we used garnet-clinopyroxene exchange thermometry to test all possible garnet-clinopyroxene inclusion combinations, and calculated temperatures range from about 1300 to 2600 °C, with five of the six pairs yielding temperatures in excess of 1700 °C using the thermometer of Nakamura (2009) (Table 2). With the possible

exception of one pair, the improbably high temperatures indicate that inclusion pairs do not represent equilibrium assemblages, which is not surprising given that none are in physical contact.

Bailey (1999) reported the major element composition of peridotitic chrome diopside clinopyroxene xenocrysts from Dachine drill core concentrates. Three of these xenocrysts have major element compositions indicating a plausible origin in garnet lherzolite, allowing single grain clinopyroxene pressure-temperature estimates based on the thermobarometer of Nimis and Taylor (2000). Thermobarometry yields a range of pressures and temperature from ~ 900 ^{o}C at ~ 2.2 GPa to ~1300 ^{o}C at ~ 5.8 GPa (Fig. 9), close to a 45 mW/m^2 geotherm; with limited samples we prefer to use these data as indicative rather than describing a particular geotherm. The highest pressure xenocrystic pyroxene suggests it was sampled in the mantle at a depth of ~180 km. On the basis of the single majoritic garnet inclusion, and assuming that all the diamonds formed deeper than the mantle xenocrysts, we estimate depths of ~ 200 to 250 km for the origin of the Dachine diamonds.

3.4.4 Coesite

A single inclusion of SiO_2, presumably coesite, is present in one Dachine diamond. The presence of a free silica phase is consistent with the eclogitic character of the garnet and clinopyroxene inclusions.

3.4.5 Sulfides

Sulfide inclusions in eighteen diamonds were analysed for major and minor elements, and their compositions are provided in Table 4 and shown in figure 10. Single-phase inclusions are pyrrhotite, and are low in Ni and Cr. In seven sulphide inclusions pyrrhotite and pentlandite coexist, with textures indicative of unmixing from a monosulfide solid solution. Two composite inclusions contain pyrrhotite and chalcopyrite. On the basis of the overall low Ni, and extremely low Cr

contents of single-phase and composite inclusions, the sulfides are consistent with an origin related to olivine-free, eclogitic protoliths rather than peridotite (Stachel and Harris, 2008).

4. Discussion

4.1 Diamond Growth Conditions

The external and internal morphology of the Dachine diamonds exhibit a monocrystalline nature. Cartigny (2010) suggested that Dachine diamonds could be related to carbonado on the basis of a similarity in C- and N- stable isotope compositions (Fig. 4), N contents and aggregation state. However, Dachine diamonds are monocrystalline, not polycrystalline like carbonado, framesite, or diamondite (Heaney et al., 2005), suggesting a different mode of formation.

The common step-layered, octahedral, external morphology of Dachine diamonds can be explained as a layer-by-layer growth process originating at a "layer nucleus" and spreading out as an advancing step to form the octahedral face of the crystal (Wentorf, 1970). If carbon supersaturation is low and relatively constant, the growing octahedral face will be flat and smooth. When carbon supersaturation is higher and fluctuating, instead of a smooth octahedral face some new layer-nuclei will form resulting in stepped growth. Although such step-layered morphology is not uncommon in lithospheric diamonds, we observe that it predominates in Dachine stones.

The internal structures of the Dachine diamonds (e.g. blocky, sectorial, granular growth structures) also indicate nucleation from liquids with a moderate to high degree of carbon supersaturation (Sunagawa, 1984), with features indicating fast growth rate in relatively restricted space. In contrast, typical lithospheric diamonds exhibit octahedral layer-by-layer growth, a mechanism consistent with a slow growth rate from fluids with a low degree of carbon supersaturation in unrestricted space (Sunagawa, 1984). Dachine diamond precipitation likely occurred from percolating fluids, with restricted delivery of carbon to the growing diamond faces in a process similar to those proposed for metamorphic and metasomatic minerals (Grigor'yev and Jabin, 1975).

Conditions during the final stages of Dachine growth, as represented by thin octahedral rims, resemble those of their lithospheric counterparts. The lack of dissolution producing dodecahedroid shapes indicates quick transportation of Dachine diamonds to the surface, in the course of which they were heavily etched.

The plastic deformation apparent in some Dachine diamonds implies high stress conditions during growth. We conclude that the external and internal morphology of Dachine diamonds are more complex than typically observed in lithospheric diamonds, and suggest growth under more dynamic conditions. Similar complex internal features and evidence of residence under stress are commonly observed in sub-lithospheric diamonds from Brazil (Bulanova et al., 2010).

4.2 Source of the Diamond-Forming Carbon

On average, the C and N isotope values for crustal and mantle derived samples are distinguishable (Boyd et al., 1994; Cartigny, 2005). The distribution of $\delta^{13}C$ and $\delta^{15}N$ values of Dachine diamonds displays a very strong similarity with the global database for Precambrian organic matter in meta-sedimentary rocks (Fig. 4). Of the samples investigated, no Dachine diamonds show coupled $\delta^{13}C$-$\delta^{15}N$ consistent with the mean mantle, a rare feature among diamond populations even when considering eclogitic monocrystalline diamonds (Cartigny, 2005). There are no other known monocrystalline diamond populations that match the coupled $\delta^{13}C$-$\delta^{15}N$ values for diamonds from Dachine, but their distribution is most similar to that of polycrystalline diamondites, although extending to more ^{13}C depleted compositions. The lack of any covariant trends among the $\delta^{13}C$, $\delta^{15}N$, and N contents in Dachine diamonds is inconsistent with a model of progressive high-temperature stable isotope fractionation (Rayleigh-type) away from initial mantle C and N isotopic values, suggesting that the diamonds have preserved the primary or near-primary isotopic compositions of the carbon source.

Evidence for the input of inorganic sedimentary carbon is found in samples DAC101Y and DAC101W, which show heavy $\delta^{13}C$ values > 0 per mil, akin to inorganic carbonate (Fig. 4).

Indeed, the two extreme groupings for $\delta^{13}C$ values (<-20 per mil vs. >0 per mil) are consistent with a carbon source that is isotopically indistinguishable from organic and inorganic sedimentary carbon that have been effectively constant throughout the geological record (Shields and Veizer, 2002; Schidlowski, 2001), and which are distinct from the MORB source (Deines, 2002).

In summary, the C and N isotopes provide evidence that the source of the carbon in Dachine diamonds is likely to be carbonaceous sediment, which would have been subducted to depths of the diamond stability field. This observation, together with the eclogitic major element chemistry of the mineral inclusions and the deformation texture of the diamonds, suggests that diamond formation occurred within the dynamic region of the slab-mantle interface, where mafic crust and oceanic sediments are juxtaposed.

4.3 Nitrogen Aggregation and Diamond Thermal History

Because increasing aggregation time and increasing temperature both lead to enhanced aggregation of C to A defects for a given total N concentration, it is not possible to use the FTIR data alone to define a unique temperature-time path. However, if all the diamonds have experienced the same thermal history, a single thermal isopath line should apply to all the data with different N concentrations. We fitted such an isopath to our data and it is shown in figure 11a, and within the uncertainties in fitting the FTIR spectra of these low N samples, it is reasonable to treat the diamonds as a group with a single thermal path involving growth, transport within the mantle, exhumation by a melt, and cooling at the surface. This thermal isopath is calculated using the slowest probable C to A kinetics with values of lnA = 18.8 and Ea = 6.0 eV (Taylor et al., 1996). The faster rate observed in the octahedral growth zones of synthetic Type Ib diamonds is widely attributed to the presence of Ni- and Co-related defects derived from the metallic solvent-catalyst used in the manufacturing process (Fisher and Lawson, 1998), and is therefore unlikely to be appropriate here. The isopath in figure 11a will be used as a test of potential models for the growth and exhumation of the Dachine diamonds. All fitting of N aggregation data with different thermal

models can be done for a single value of N concentration and aggregation on the isopath, so for simplicity we will take a value of 200 ppm N and 45%1aA, although any point along the curve would serve equally well.

The simplest thermal model is to assume that diamonds had a fixed temperature during the time interval between their growth and exhumation. Fig 11b shows the interplay between time and temperature for the isopath and illustrates how timescales vary enormously for relatively modest differences in temperature. For example at a fixed temperature of 800°C it would take 13 Ga to achieve the observed N aggregation, but at 1000 °C it would take only 0.5 Ma and at 1300°C it would take just 15 years. On the basis of the thermobarometry described in section 3.4.3, the diamonds likely formed in the depth range of ~200 to 250 km. If the diamonds formed in convecting mantle at such depths, as has been previously suggested on the basis of an assumed komatiite host (Capdevila et al., 1999; Cartigny, 2010), then for a 1400 °C mantle potential temperature, the mantle temperature at such depths would be ~ 1550 °C. The time required for N aggregation at that temperature is twelve days. The temperature expected for nominally anhydrous komatiite formation at this depth in the mantle is greater than 1700 °C (Walter, 1998), implying aggregation in about two hours. This analysis effectively precludes derivation of the diamonds in ambient mantle, and makes hot komatiite an unlikely host.

This approach can be made more sophisticated by combining different thermal steps for growth and transport of the diamonds through the mantle. On the basis of our deductions from inclusion chemistry and diamond isotopic compositions, it is instructive to consider thermal regimes associated with subduction of oceanic crust, specifically in the region of the slab-mantle interface (see more detailed discussion in section 4.5.1). For example, consider a path where the diamonds experienced temperatures in the range of 800-1300 °C; the lower end of the range reflects a possible temperature at the slab-mantle interface at ~ 200-250 km depth (Syracuse et al., 2010), whereas the higher end of the range is the temperature recorded by the xenocrystic pyroxene. (Fig. 9). For simplification, temperature is assumed to increase linearly with time over the duration of the

isopath. For such a model the residence time is ~100 years. If we reduce the maximum temperature to 1100 °C, then the residence time increases to about 100,000 years. Of course many other models can be constructed with longer residence time at lower temperature and short residence time at higher temperature (e.g. in the host magma). What is clear from Figure 11 is that the N aggregation states of Dachine diamonds record temperature-time paths that effectively precludes any protracted (e.g. > ~1 Ma) high temperature (e.g. >1000 °C) thermal history.

4.4 Silicate Inclusion Petrogenesis

As described above, the inclusions in Dachine diamonds are distinctly mafic in character, and indicate an eclogitic protolith. They also show unusual trace element characteristics such as extreme depletions in some incompatible elements (e.g. LREE) but enrichments in trace metals (e.g. Ni, Co and Mn). Here we use forward modelling to test whether the trace element compositions of the silicate inclusions are generally consistent with our observations indicating that the diamonds and inclusions are intimately related with subducted oceanic crust, and formed at the slab-mantle interface.

Modelling mineral phase equilibria and partitioning along a subduction zone P-T path involving metamorphism, dehydration and/or melting, requires numerous assumptions and choices. To model the rare earth elements, we have chosen the element partitioning and phase equilibrium results of Kessel et al at 6 GPa (Kessel et al., 2005a; Kessel et al., 2005b) to test whether a garnet + clinopyroxene ± liquid assemblage with the bulk REE content of subducted normal MORB can account to first-order for the observed abundances in the Dachine inclusions. Kessel et al provide partitioning data at both 800 and 1000 °C for garnet and clinopyroxene in equilibrium with supercritical fluids, and REE partition coefficients can vary by up to an order of magnitude between these temperatures. Here we present models based on the 800 °C data as this temperature better coincides with model temperatures of the slab-mantle interface at the depths at which dehydration

occurs (~100 – 200 km) (e.g. Syracuse et al, 2010). We note, however, that our interpretations based on the modelling are not affected substantially by this choice.

We begin by considering a simple garnet-clinopyroxene lithology. Figure 12 shows that the inclusion REE abundances are not consistent with this mineralogy in a normal MORB composition; the Dachine garnet and clinopyroxene inclusions are far too depleted in LREE, and the garnets are too enriched in HREE. Next we tested models for a garnet-clinopyroxene mineralogy residual to liquid extraction. We found that no combination of degree of extraction or mineral modes could provide a reasonable match to the observed patterns using the Kessel et al data, most notably the extreme depletion in the LREE. On this basis, we conclude that for a MORB type source, the Dachine inclusions indicate a role for another phase, one with a marked preference for the LREE.

In eclogite–facies rocks, minor phases such as monazite, epidote or allanite can dominate the REE budget of co-existing solids and liquids (e.g. Hermann, 2002; Scambelluri and Philippot, 2001; Skora et al, 2010). Tribuzio et al (1996) and Hermann (2002) observed allanite in alpine eclogite facies rocks, and epidote–zoisite is common in exhumed ultra-high-pressure eclogitic terrains (Enami et al, 2004). Hermann (2002) and Klimm et al (2008) show a wide stability region for allanite above the solidus during hydrous melting of MORB at 4.5 and 2.5 GPa, respectively. In their study of hydrous melting of normal MORB at 3 GPa, Carter et al (2015) did not stabilize allanite, but instead found epidote in equilibrium with hydrous melt/fluid to at least 900 °C. These authors attributed the presence of allanite in previous studies to high doping levels of the REE, and suggest that in natural subducted eclogite epidote is the more likely REE carrying trace phase.

Epidote and allanite both have an extreme preference for the LREE, and small amounts of either can generate large depletions in coexisting garnet and clinopyroxene. Here we use the mineral/liquid partition coefficients from Klimm et al (2008) for allanite as a proxy for an REE rich trace phase, as these authors provide a nearly full set of coefficients. We note that the epidote/liquid partition coefficients of Carter et al for the LREE are very similar to those of Klimm et al for

allanite (e.g. 1470 and 1598 for La, respectively), so that the choice of phase has only a small effect on the model outcome. Figure 12 shows that a much better fit to the Dachine inclusions can be obtained, for example, when a small amount of allanite is included in the equilibrium assemblage (e.g. ~ 0.5 - 1%). The abundance pattern does not change appreciably if liquid extraction is included in the model. We have tested many scenarios, and the overall result is that the Dachine garnet and clinopyroxene inclusion REE concentrations can, in principle, be explained by equilibration among garnet, clinopyroxene, a liquid and an LREE-enriched trace accessory phase such as epidote or allanite.

We now extend our modelling to other transition metal elements, as shown in figure 13. Again, a simple subducted MORB lithology of garnet and clinopyroxene cannot account for the observed abundances, with notable enrichments in Mn, Ni and Co and depletions in Nb, Zr, Hf and Ti. The enriched Mn, Ni, and Co inclusion compositions would seem to require an unusual component in the bulk composition of the protolith. We posit above that the C and N isotopic compositions of the Dachine diamond indicate a subducted sediment contribution. Within that context, a plausible explanation is sediment enriched in Mn and other metals.

To model the effect of a sediment component, we simulate metalliferous sediment using average Mn-Fe concentrations in hydrothermal crusts of the world oceans and in hydrothermal crusts of the northwestern Pacific (Anikeeva et al., 2003; Baturin et al., 2012; Usui and Someya, 1997), which are given as Av-1 and Av-2 in Baturin et al. (2012). These compositions are also representative of ferromanganese crusts from the sea of Okhotsk (Baturin et al., 2012), as well as those from the East Pacific seafloor (Toth, 1980). We find that it requires the addition of ~10 to 20% of such a sediment to account for the Mn and Ni contents of the silicates. This addition causes some ancillary enrichment in other incompatible lithophile elements as well, but this is a minor effect, as shown for the REE in figure 12.

While our model of MORB plus subducted metalliferous sediment can match the metal and REE abundances observed in the inclusions reasonably well, none of our models match the observed depletions in Nb, Zr, Hf and Ti in the inclusions. These depletion require another phase that partitions these elements strongly, such as rutile. Nb, Ta, Ti, Zr and Hf are notably depleted in subduction zone magmas relative to MORB, and residual rutile is considered a likely host (Foley et al., 2000; Hermann and Rubatto, 2009; Klemme et al., 2005). Experiments show that rutile can be stable in subducted crustal protoliths over a wide range of pressure-temperature conditions and in the presence of melts and fluids, and that although these elements are compatible in rutile, partition coefficients vary considerably as a function of pressure, temperature and composition (Bromiley and Redfern, 2008; Foley et al., 2000; Hermann and Rubatto, 2009; Klemme et al., 2005; Klimm et al., 2008; Schmidt et al., 2004). Figure 13 shows that rutile can in principle generate the observed depletions, but it would require of the order 5-10% rutile in the mode using the most compatible set of partitioning coefficients. However, rutile cannot produce the very high Ta/Nb ratios found in two of the garnet inclusions.

In summary, Dachine silicate inclusion trace element abundances are not consistent with a garnet + clinopyroxene MORB eclogite mineralogy, but require the addition of accessory phases that preferentially partition LREE and (e.g. epidote) and high field strength elements (e.g. rutile). The high Mn, Ni and Co contents of the inclusions require a unique source enriched in these elements, and especially Mn, and modelling indicates that 10-20% of subducted ferromanganese crust can provide a reasonable match. It is noteworthy that the age of the diamond host rock at ~2.2 Ga correlates generally with the onset of a pulse of volcanogenic massive sulfide deposition, banded iron formation and crustal growth extending into the Neoproterozoic (Bekker et al., 2004).

4.5 A Model for the Petrogenesis of Dachine Diamonds

The observations and deductions presented above indicate that diamond and inclusion formation is intimately linked with subducted mafic crust. The data indicate that this occurred in the region of

the slab-mantle interface at depths of ~ 200 to 250 km, and involved an eclogitic protolith with some contribution from a metal-rich sediment. In this section we develop a petrogenetic model for the diamonds, their inclusions, and the host magma, which attempts to combine all our observations.

4.5.1 Subduction Zone Thermal Structure and Depth of Diamond Formation

The thermal modeling of Syracuse et al (2010) yields a wide range of pressure-temperature paths for modern subduction zones. In these models, slab surface and interior (e.g. at the slab Moho) temperatures depend on factors including slab age, convergence velocity, depth of partial coupling of slab and plate, and the wedge thermal profile, among others. We infer that Proterozoic subduction zones had similar ranges in these parameters as observed today, so we expect a similar thermal variability. The slab surface reaches the 800 °C isotherm in nearly all models by Syracuse et al at depths from ~80 km to 150 km. By 250 km the slab surface is expected to be higher, reaching up to ~1100 °C and with most > 900 °C. Slab crust and sediments are predicted to dehydrate considerably (e.g. to < 0.5 wt% water) by ~ 700 °C, such that the crust is essentially dehydrated by ~100 km in nearly all cases considered (e.g. below the volcanic front and responsible for primary arc magmatism); this depth is too shallow for diamond formation at slab-surface temperatures. In some colder subduction zone models dehydration extends to at least ~150 km. At 900 °C diamond becomes stable at ~ 140 km (Bundy, 1989). As discussed above, we suggest Dachine diamonds form at the slab-mantle interface in a depth range between about 200 and 250 km, deeper than shallow slab dehydration, and on the basis of the thermal modeling of Syracuse et al, at temperatures in the range of ~900 to 1100 °C.

4.5.2 The Source of Carbon

The isotope data indicate that the source of C and N in Dachine diamonds is primarily sedimentary organic material, with a minor role of inorganic carbon, and if so, these components must largely survive shallow dehydration. The fate of sedimentary organic and inorganic carbon during subduction and crustal dehydration is not easily deduced, and depends on many factors including pressure, temperature, oxygen fugacity and pH.

Calcite may have considerable solubility in aqueous fluids during slab dehydration, providing a significant carbon flux to the mantle wedge and arc magmas as oxidized species (e.g. CO_2, CO_3^{2-}) (Frezzotti et al., 2011; Manning et al., 2013). Preservation of reduced organic carbon to greater depths may be more favorable. Along a subduction pressure-temperature path that leads to slab dehydration above ~ 140 km, sedimentary organic carbon will have gone through a series of metamorphic reactions that generate an array of hydrocarbons and other carbon compounds, a likely end-product of which is elemental carbon at the temperatures of crustal dehydration and higher (e.g. > 700 °C) (Bustin et al., 1995). While isotopic fractionation factors during metagenesis of sedimentary organic matter are uncertain without knowledge of the relevant reactions, they may not be large (Cook-Kollars et al., 2014). The solubility of elemental carbon in H_2O-rich fluids can be very low (Connolly, 1995; Frezzotti et al., 2011), and we suggest this is the most likely form of sedimentary carbon carried to depths greater than ~100 km at the slab mantle interface.

Solid-state conversion of graphite to diamond is kinetically inhibited in the absence of a fluid phase, and graphite may remain metastable to much greater depths (e.g. Tappert et al, 2005). Dachine diamond internal structures are not consistent with solid-state growth from residual graphitic carbon, but suggest crystallization from a carbon saturated liquid. Given that Dachine diamonds formed at depths of 200 to 250 km, we suggest they must be related to a later generation of diamond precipitation unrelated to shallow slab dehydration, which requires a deeper source for the diamond precipitating liquid.

4.5.3 The Source of the Diamond Precipitating Liquid

A significant amount of water can be delivered beyond crustal dehydration depths in serpentine or chlorite in peridotitic mantle just above the slab surface or within its interior. Chlorite in the mantle wedge directly above the slab can transport water to depths of ~ 250 km in colder slabs. Similarly, serpentine, chlorite or Phase A may transport water in the interior of colder slabs, but should break down by ~250 km (Komabayashi and Omuri, 2006; Pawley et al., 2011; Syracuse et al., 2010). We note that many of the subduction geotherms for slabs in the models of Syracuse et al lead to serpentine dehydration in the slab interior in the range of 150 to 250 km, in the range estimated for Dachine diamond formation.

We suggest that the source of the Dachine diamond precipitating liquid is deserpentinization of slab peridotite. The exact composition of the aqueous liquids released from serpentinite at these deep slab conditions is not known, but they are likely to be oxidizing because ferric iron released during the breakdown of serpentine minerals does not partition into residual olivine and enstatite (Debret et al., 2014). Experiments show that a wide variety of liquid compositions can provide suitable media for diamond growth, including oxidizing carbonated and carbo-silicate liquids, and carbon saturated sulfide melts (see review in Shirey et al., 2013). The relatively common occurrence of sulfide inclusions in Dachine diamonds suggests a role for sulfur, and the eclogitic character of the sulfides (low Ni and Cr) and silicate inclusions indicates that precipitation of diamond did not occur within peridotite, but within an olivine-free, eclogitic lithology.

4.5.4 Remobilisation of Carbon and Precipitation of Diamond at the Slab-Mantle Interface

Calculated carbon speciation in high pressure-temperature liquids equilibrated with eclogitic mineral assemblages at depths greater than 150 km indicate that reaction with elemental carbon (e.g. graphite or diamond) and oxidizing aqueous liquids can lead to stabilization of methane, bicarbonate, CO_2, or other aqueous organic species such as acetic acid or acetate (Sverjensky et al., 2014). We suggest that such liquids, percolating along the slab mantle interface, may dissolve and remobilize subducted sedimentary carbon, which as discussed above will be in the form of

metastable-graphite or diamond at depths in our preferred range of 200 – 250 km. Subsequent changes in liquid composition as the liquids migrate and react, including changes in pH and/or fO_2, may lead to carbon saturation and diamond precipitation. For example, a fluid containing acetate and carbonate that undergoes a pH change associated with metasomatic reactions in eclogite or metasediment can precipitate diamond (Sverjensky et al., 2014). Growth features of Dachine diamonds are consistent with precipitation from a carbon supersaturated liquid (section 4.1), and this may occur when carbon-bearing liquids are driven to carbon supersaturation by reaction with eclogite.

4.5.5 The Relationship Between Diamond Formation and the Host Magma

The non-aggregated state of N in Dachine diamonds suggests a short residence time before transport to the surface in the host magma, which implies a close relationship in space and time between the host magma and the diamond forming metasomatic processes occurring at the slab-mantle interface. We speculate that the generation of the primary Dachine ultramafic melt is also related to deserpentinisation in the slab. Hydrous liquids supplied by deserpentinisation can percolate into wedge peridotite just above the slab-mantle interface. Experiments show that water-saturated melting of fertile peridotite can produce ultramafic liquids at temperatures as low as ~1050 °C at 150 to 250 depth (Kawamoto and Holloway, 1997), or possibly at even lower temperatures (Grove et al, 2006). The experimental melt compositions of Kawamoto and Holloway at 5 and 7.5 GPa are qualitatively akin to the Dachine host rock composition in terms of MgO, SiO_2 and FeO. Mobilisation and migration of hydrous ultramafic melts may occur in compaction channels within the rheological boundary at the slab mantle interface (Wilson et al., 2014), and may entrain diamonds formed in this region by earlier metasomatic reactions also caused by slab deserpentinisation. The volatile-rich melts would then be required to transit some pathway through mantle wedge with their diamond cargo, heating as they go and causing further flux melting, akin to the model presented in Grove et al (2006). If the pressures and temperatures of the clinopyroxene

xenocrysts are reliable, the indication is that the melts reached temperatures in the mantle wedge of ~1300 °C. Heating to such temperatures would substantially decrease the time interval permitted between diamond formation and host melt segregation, perhaps to the order of hundreds or thousands of years.

5. Conclusions

Our observations show that Dachine diamonds and their mineral inclusions have a range of characteristics that are unique among known populations of diamonds. The geological setting, host rock, isotopic signature and inclusion mineral chemistry all point to a subduction zone environment for their genesis. On the basis of garnet inclusion and clinopyroxene xenocryst barometry we suggest a depth of origin of ~200-250 km. The unique C and N isotopic composition of the diamonds indicates growth from carbon with a distinctly character, possibly deposited as organic matter plus carbonate on an early Proterozoic seafloor. The highly depleted incompatible element abundances in the silicate inclusions are consistent with their derivation in an eclogitic assembly containing trace phases such as epidote and rutile, whereas the unusual enrichments in Mn, Ni and Co in the silicate inclusions can be explained by a sediment component akin to average worldwide ferromanganese rich crust deposited on the ocean floor. The Dachine diamonds may have grown at the slab mantle interface at 200-250 km and ~800-1000 °C from liquids derived by deserpentinization of subducted peridotite. These liquids may have remobilized subducted sedimentary carbon and reprecipitated diamond. Deep slab dehydration may also have resulted in water-saturated melting of peridotite in mantle just above the slab-mantle interface generating a hydrous ultramafic host magma that entrained the diamonds as the melt migrated from its source area. Although temperature-time paths cannot be well constrained, the non-aggregated nature of N defects in Dachine diamonds indicates that the entire process may have occurred in a geologically short time frame, perhaps of the order of $10^2 – 10^6$ years.

Acknowledgements. Rio Tinto is thanked for provision of diamonds from prospecting operations, and for permission to publish. This research was supported by NERC grant NE/J008583/1 to MJW and SCK. Stuart Kearns (Bristol) and Richard Hinton (EIMF) are thanked for expert assistance with electron and ion microprobe measurements. S. Aulbach and K. Smart are thanked for thoughtful and thorough reviews that considerably improved the manuscript, and S. Shirey and F. Nestola are thanked for expert editorial handling.

References

Allen, B.P., Evans, T., 1981. Aggregation of nitrogen in diamond, including platelet formation. Proceedings of the Royal Society of London Series a-Mathematical Physical and Engineering Sciences 375, 93-104.

Anikeeva, L.I., Andreev, S.I., Kazakova, V.E., 2003. Cobalt rich ores of the worlds oceas, Vniiokean Geologiya, St. Petersburg.

Aulbach, S., Stachel, T., K.S., V., Brey, G.P., Harris, J.W., 2002. Eclogitic and websteritic diamond sources beneath the limpopo belt – is slab-melting the link? Contributions to Mineralogy and Petrology 143, 56-70.

Bailey, L.M., 1999. An unusual diamond-bearing talc schist from the dachine area of french guiana. Queen's University, Kingston, Ontario, Canada, p. 159.

Baturin, G.N., Dubinchuk, V.T., Rashidov, V.A., 2012. Ferromanganese crusts from the sea of Okhotsk. Oceanology 52, 88-100.

Bekker, A., Holland, H.D., Wang, P.L., Rumble, D., Stein, H.J., Hannah, J.L., Coetzee, L.L., Beukes, N.J., 2004. Dating the rise of atmospheric oxygen. Nature 427, 117-120.

Bottrill, R.S., 2004. Garnet-bearing and other spotted porphyroblastic metasedimentary rocks from the Balfour area. Mineral Resources Tasmania, Tasmanian Geological Survey Record 2004/02, pp. 1-8.

Boyd, S.R., Pineau, F., Javoy, M., 1994. Modeling the growth of natural diamonds. Chemical Geology 116, 29-42.

Brenker, F.E., Vollmer, C., Vincze, L., Vekemans, B., Szymanski, A., Janssens, K., Szaloki, I., Nasdala, L., Joswig, W., Kaminsky, F., 2007. Carbonates from the lower part of transition zone or even the lower mantle. Earth and Planetary Science Letters 260, 1-9.

Bromiley, G.D., Redfern, S.A.T., 2008. The role of TiO_2 phases during melting of subduction-modified crust: Implications for deep mantle melting. Earth and Planetary Science Letters 267, 301-308.

Bulanova, G.P., 1995. The formation of diamond. Journal of Geochemical Exploration 53, 1-23.

Bulanova, G.P., Pearson, D.G., Hauri, E.H., Griffin, B.J., 2002. Carbon and nitrogen isotope systematics within a sector-growth diamond from the Mir kimberlite, Yakutia. Chemical Geology 188, 105-123.

Bulanova, G.P., Shelkov, D., Milledge, H.J., Hauri, E.H., Smith, C.B., 1999. Nature of eclogitic diamonds from Yakutian kimberlites: Evidence from isotopic composition and chemistry of inclusions, in: J.J.Gurney, J.L.G., M.D. Pascoe, and S.H.Richardson (Eds) (Ed.), Proceedings of the 7th International Kimberlite Conference. Red Roof Design, Capetown, pp. 57-65.

Bulanova, G.P., Varshavsky, A.V., Kotegov, V.A., 2005. A venture into the interior of natural diamond: Genetic information and implications for the gem industry. Part 1: The main types of internal growth structures. Journal of Gemmology 29, 377-386.

Bulanova, G.P., Walter, M.J., Smith, C.B., Kohn, S.C., Armstrong, L.S., Blundy, J., Gobbo, L., 2010. Mineral inclusions in sublithospheric diamonds from Collier 4 kimberlite pipe, Juina, Brazil: Subducted protoliths, carbonated melts and primary kimberlite magmatism. Contributions to Mineralogy and Petrology 160, 489-510.

Bundy, F.P., 1989. Pressure-temperature phase-diagram of elemental carbon. Physica A 156, 169-178.

Bustin, R.M., Ross, J.V., Rouzaud, J.N., 1995. Mechanisms of graphite formation from kerogen - experimental-evidence. International Journal of Coal Geology 28, 1-36.

Capdevila, R., Arndt, N., Letendre, J., Sauvage, J.F., 1999. Diamonds in volcaniclastic komatiite from French Guiana. Nature 399, 456-458.

Carter, L.B., Skora, S., Blundy, J.D., De Hoog, J.C.M., Elliott, T., 2015. An experimental study of trace element fluxes from subducted oceanic crust. Journal of Petrology 56, 1585-1605.

Cartigny, P., 2005. Stable isotopes and the origin of diamond. Elements 1, 79-84.

Cartigny, P., 2010. Mantle-related carbonados? Geochemical insights from diamonds from the Dachine komatiite (French Guiana). Earth and Planetary Science Letters 296, 329-339.

Cartigny, P., Boyd, S.R., Harris, J.W., Javoy, M., 1997. Nitrogen isotopes in peridotitic diamonds from Fuxian, China: The mantle signature. Terra Nova 9, 175-179.

Cartigny, P., Harris, J.W., Javoy, M., 1998. Eclogitic diamond formation at Jwaneng: No room for a recycled component. Science 280, 1421-1424.

Cartigny, P., Harris, J.W., Javoy, M., 1999. Peridotitic and metamorphic diamonds and the problems of carbon recycling—the case of Orapa (Botswana), 7th International Kimberlite Conference Extended Abstract, pp. 117-124.

Cartigny, P., Stachel, T., Harris, J.W., Javoy, M., 2004. Constraining diamond metasomatic growth using C- and N-stable isotopes: Examples from Namibia. Lithos 77, 359-373.

Collerson, K.D., Williams, Q., Kamber, B.S., Omori, S., Arai, H., Ohtani, E., 2010. Majoritic garnet: A new approach to pressure estimation of shock events in meteorites and the encapsulation of sub-lithospheric inclusions in diamond. Geochimica Et Cosmochimica Acta 74, 5939-5957.

Connolly, J.A.D., 1995. Phase-diagram methods for graphitic rocks and application to the system C-O-H-FeO-TiO_2-SiO_2. Contributions to Mineralogy and Petrology 119, 94-116.

Cook-Kollars, J., Bebout, G.E., Collins, N.C., Angiboust, S., Agard, P., 2014. Subduction zone metamorphic pathway for deep carbon cycling: I. Evidence from hp/uhp metasedimentary rocks, Italian Alps. Chemical Geology 386, 31-48.

Debret, B., Andreani, M., Munoz, M., Bolfan-Casanova, N., Carlut, J., Nicollet, C., Schwartz, S., Trcera, N., 2014. Evolution of Fe redox state in serpentine during subduction. Earth and Planetary Science Letters 400, 206-218.

Deines, P., 2002. The carbon isotope geochemistry of mantle xenoliths. Earth-Science Reviews 58, 247-278.

Dobosi, G., Kurat, G., 2010. On the origin of silicate-bearing diamondites. Mineralogy and Petrology 99, 29-42.

Dube, B., Mercier-Langevin, P., Hannington, M., Lafrance, B., Gosselin, G., Gosselin, P., 2007. The LaRonde Penna world-class au-rich volcanogenic massive sulfide deposit, Abitibi, Quebec: mineralogy and geochemistiy of alteration and implications for genesis and exploration. Economic Geology 102, 633-666.

Enami, M., Liou, J.G., Mattinson, C.G., 2004. Epidote minerals in high p/t metamorphic terranes: Subduction zone and high- to ultrahigh-pressure metamorphism. Reviews In Mineralogy and Geochemistry 56: Epidotes, 347-398.

Fisher, D., Lawson, S.C., 1998. The effect of nickel and cobalt on the aggregation of nitrogen in diamond. Diamond and Related Materials 7, 299-304.

Foley, S.F., Barth, M.G., Jenner, G.A., 2000. Rutile/melt partition coefficients for trace elements and an assessment of the influence of rutile on the trace element characteristics of subduction zone magmas. Geochimica Et Cosmochimica Acta 64, 933-938.

Frezzotti, M.L., Selverstone, J., Sharp, Z.D., Compagnoni, R., 2011. Carbonate dissolution during subduction revealed by diamond-bearing rocks from the alps. Nature Geoscience 4, 703-706.

Fritsch, E., Hainschwang, T., Massi, L., Rondeau, B., 2007. Hydrogen-related optical centers in natural diamond: An update. New Diamond and Frontier Carbon Technology 17, 63-89.

Gautheron, C., Cartigny, P., Moreira, M., Harris, J.W., Allegre, C.J., 2005. Evidence for a mantle component shown by rare gases, C and N isotopes in polycrystalline diamonds from Orapa (Botswana). Earth and Planetary Science Letters 240, 559-572.

Grigor'yev, A.G., Jabin, A.G., 1975. Ontogeniya of minerals. Nauka, Moscow.

Grove, T.L., Chatterjee, N., Parman, S.W., Medard, E., 2006. The influence of H_2O on mantle wedge melting. Earth and Planetary Science Letters 249, 74-89.

Gruau, G., Martin, H., Leveque, B., Capdevila, R., Marot, A., 1985. Rb-Sr and Sm-Nd geochronology of lower proterozoic granite greenstone terrains in French Guiana, South-America. Precambrian Research 30, 63-80.

Gurney, J.J., Helmstaedt, H.H., Richardson, S.H., Shirey, S.B., 2010. Diamonds through time. Economic Geology 105, 689-712.

Haggerty, S.E., 1999. Earth and planetary sciences - a diamond trilogy: Superplumes, supercontinents, and supernovae. Science 285, 851-860.

Hainschwang, T., Fritsch, E., Notari, F., Rondeau, B., 2012. A new defect center in type Ib diamond inducing one phonon infrared absorption: The Y center. Diamond and Related Materials 21, 120-126.

Hardy, J.R., Smith, S.D., 1961. 2-phonon infra-red lattice absorption in diamond. Philosophical Magazine 6, 1163-1172.

Harte, B., 2010. Diamond formation in the deep mantle: The record of mineral inclusions and their distribution in relation to mantle dehydration zones. Mineralogical Magazine 74, 189-215.

Harte, B., Harris, J.W., Hutchison, M.T., Watt, G.R., Wilding, M.C., 1999. Lower mantle mineral associations in diamonds from Sao Luiz, Brazil. in Mantle Petrology: Field observations and high pressure experimentation (eds: Fei, Y., Bertka, C. M. and Mysen, B. O.) Geochemical Society Special Publications, 125-153.

Heaney, P.J., Vicenzi, E.P., De, S., 2005. Strange diamonds: The mysterious origins of carbonado and framesite. Elements 1, 85-89.

Hermann, J., 2002. Allanite: Thorium and light rare earth element carrier in subducted crust. Chemical Geology 192, 289-306.

Hermann, J., Rubatto, D., 2009. Accessory phase control on the trace element signature of sediment melts in subduction zones. Chemical Geology 265, 512-526.

Kawamoto, T., Holloway, J.R., 1997. Melting temperature and partial melt chemistry of H_2O-saturated mantle peridotite to 11 gigapascals. Science 276, 240-243.

Kessel, R., Schmidt, M.W., Ulmer, P., Pettke, T., 2005a. Trace element signature of subduction-zone fluids, melts and supercritical liquids at 120-180 km depth. Nature 437, 724-727.

Kessel, R., Ulmer, P., Pettke, T., Schmidt, M.W., Thompson, A.B., 2005b. The water-basalt system at 4 to 6 GPa: Phase relations and second critical endpoint in a K-free eclogite at 700 to 1400 degrees C. Earth and Planetary Science Letters 237, 873-892.

Klein, E.M., 2003. Geochemistry of the igneous oceanic crust, in: Holland, H.D., Turekian, K.K. (Eds.), Treatise on geochemistry. Elsevier B.V., p. 433.

Klein-BenDavid, O., Pearson, D.G., Nowell, G.M., Ottley, C., McNeill, J.C.R., Cartigny, P., 2010. Mixed fluid sources involved in diamond growth constrained by Sr-Nd-Pb-C-N isotopes and trace elements. Earth and Planetary Science Letters 289, 123-133.

Klemme, S., Prowatke, S., Hametner, K., Gunther, D., 2005. Partitioning of trace elements between rutile and silicate melts: Implications for subduction zones. Geochimica Et Cosmochimica Acta 69, 2361-2371.

Klimm, K., Blundy, J.D., Green, T.H., 2008. Trace element partitioning and accessory phase saturation during H_2O -saturated melting of basalt with implications for subduction zone chemical fluxes. Journal of Petrology 49, 523-553.

Komabayashi, T., Omori, S., 2006. Internally consistent thermodynamic data set for dense hydrous magnesium silicates up to 35 GPa, 1600 degrees C: Implications for water circulation in the earth's deep mantle. Physics of the Earth and Planetary Interiors 156, 89-107.

Lawson, S.C., Fisher, D., Hunt, D.C., Newton, M.E., 1998. On the existence of positively charged single-substitutional nitrogen in diamond. Journal of Physics-Condensed Matter 10, 6171-6180.

Magee, C.W., 2001. Geologic, microstructural, and spectroscopic constraints on the origin and history of carbonado diamond. Australian National University, Canberra, Australia.

Magee, C.W., Taylor, W.R., 1999. Diamond and chromite geochemical constraints on the nature of the dachine complex, French Guiana, Annual Report. Australian National University, Canberra, Australia, p. 85.

Manning, C.E., Shock, E.L., Sverjensky, D.A., 2013. The chemistry of carbon in aqueous fluids at crustal and upper-mantle conditions: Experimental and theoretical constraints, in: Hazen, R.M., Jones, A.P., Baross, J.A. (Eds.), Carbon in Earth, pp. 109-148.

McCandless, T.E., Letendre, J., Eastoe, C.J., 1999. Morphology and carbon isotope composition of microdiamonds from Dachine, French Guiana, in: J.J. Gurney, J.L. Gurney, M.D. Pascoe, & S.H. Richardson (Ed.), 7th International Kimberlite Conference, Cape Town, pp. 550-556.

McDonough, W.F., Sun, S.S., 1995. The composition of the earth. Chemical Geology 120, 223-253.

Melcher, F., 1995. Genesis of chemical sediments in Birimian greenstone belts - evidence from gondites and related manganese-bearing rocks from northern Ghana. Mineralogical Magazine 59, 229-251.

Meyer, H.O.A., 1987. Inclusions in diamond, in: Nixon, P.H. (Ed.), Mantle xenoliths. John Wiley and Sons Ltd, Chichester, pp. 501-522.

Mikhail, S., Dobosi, G., Verchovsky, A.B., Kurat, G., Jones, A.P., 2013. Peridotitic and websteritic diamondites provide new information regarding mantle melting and metasomatism induced through the subduction of crustal volatiles. Geochimica Et Cosmochimica Acta 107, 1-11.

Mikhail, S., Verchovsky, A.B., Howell, D., Hutchison, M.T., Southworth, R., Thomson, A.R., Warburton, P., Jones, A.P., Milledge, H.J., 2014. Constraining the internal variability of the stable isotopes of carbon and nitrogen within mantle diamonds. Chemical Geology 366, 14-23.

Morris, T.F., Sage, R.P., Ayer, J.A., Crabtree, D.C., 2002. A study in clinopyroxene composition: Implications for kimberlite exploration. Geochemistry: Exploration, Environment, Analysis, 2, 321-331.

Nakamura, D., 2009. A new formulation of garnet-clinopyroxene geothermometer based on accumulation and statistical analysis of a large experimental data set. Journal of Metamorphic Geology 27, 495-508.

Navon, O., Hutcheon, I.D., Rossman, G.R., Wasserburg, G.J., 1988. Mantle-derived fluids in diamond micro-inclusions. Nature 335, 784-789.

Nimis, P., Taylor, W.R., 2000. Single clinopyroxene thermobarometry for garnet peridotites. Part I. Calibration and testing of a Cr-in-cpx barometer and an enstatite-in-cpx thermometer. Contributions to Mineralogy and Petrology 139, 541-554.

Pawley, A.R., Chinnery, N.J., Clark, S.M., Walter, M.J., 2011. Experimental study of the dehydration of 10A-phase, with implications for its H_2O content and stability in subducted lithosphere. Contributions to Mineralogy and Petrology 162, 1279-1289.

Pearson, D.G., Wittig, N., 2008. Formation of Archaean continental lithosphere and its diamonds: The root of the problem. Journal of the Geological Society 165, 895-914.

Pertermann, M., Hirschmann, M.M., Hametner, K., Gunther, D., Schmidt, M.W., 2004. Experimental determination of trace element partitioning between garnet and silica-rich liquid during anhydrous partial melting of morb-like eclogite. Geochemistry Geophysics Geosystems 5, doi:10.1029/2003GC000638.

Pollack, H.N., Chapman, D.S., 1977. Regional variation of heat-flow, geotherms, and lithospheric thickness. Tectonophysics 38, 279-296.

Scambelluri, M., Philippot, P., 2001. Deep fluids in subduction zones. Lithos 55, 213-227.

Schidlowski, M., 2001. Carbon isotopes as biogeochemical recorders of life over 3.8 ga of earth history: Evolution of a concept. Precambrian Research 106, 117-134.

Schmidt, M.W., Dardon, A., Chazot, G., Vannucci, R., 2004. The dependence of Nb and Ta rutile-melt partitioning on melt composition and Nb/Ta fractionation during subduction processes. Earth and Planetary Science Letters 226, 415-432.

Shelkov, D., Verkhovsky, A.B., Milledge, H.J., Pillinger, C.T., 1997. Carbonado: A comparison between Brazilian and Ubangui sources with other forms of microcrystalline diamond based on carbon and nitrogen isotopes. Geologiya I Geofizika 38, 315-322.

Shields, G., Veizer, J., 2002. Precambrian marine carbonate isotope database: Version 1.1. Geochemistry Geophysics Geosystems 3.

Shirey, S.B., Cartigny, P., Frost, D.J., Keshav, S., Nestola, F., Nimis, P., Pearson, D.G., Sobolev, N.V., Walter, M.J., 2013. Diamonds and the geology of mantle carbon, in: Hazen, R.M., Jones, A.P., Baross, J.A. (Eds.), Carbon in Earth, pp. 355-421.

Shirey, S.B., Harris, J.W., Richardson, S.H., Fouch, M.J., James, D.E., Cartigny, P., Deines, P., Viljoen, F., 2002. Diamond genesis, seismic structure, and evolution of the Kaapvaal-Zimbabwe craton. Science 297, 1683-1686.

Skora, S., Blundy, J., 2010. High-pressure hydrous phase relations of radiolarian clay and implications for the involvement of subducted sediment in arc magmatism. Journal of Petrology 51, 2211-2243.

Slack, J.F., Grenne, T., Bekker, A., 2009. Seafloor-hydrothermal Si-Fe-Nn exhalites in the Pecos greenstone belt, New Mexico, and the redox state of ca. 1720 ma deep seawater. Geosphere 5, 302-314.

Spry, P.G., Wonder, J.D., 1989. Manganese-rich garnet rocks associated with the Broken Hill lead-zinc-silver deposit, New-South-Wales, Australia. Canadian Mineralogist 27, 275-292.

Stachel, T., Aulbach, S., Brey, G.P., Harris, J.W., Leost, I., R., T., Viljoen, K.S., 2004. The trace element composition of silicate inclusions in diamonds: A review. Lithos 77, 1-19.

Stachel, T., Brey, G.P., Harris, J.W., 2005. Inclusions in sublithospheric diamonds: Glimpses of the deep earth. Elements 1, 73-78.

Stachel, T., Harris, J.W., 2008. The origin of cratonic diamonds - constraints from mineral inclusions. Ore Geology Reviews 34, 5-32.

Stachel, T., Harris, J.W., 2009. Formation of diamond in the earth's mantle. Journal of Physics-Condensed Matter 21.

Sunagawa, I., 1984. Morphology of natural and synthetic diamond crystals, in: Sunagawa, I. (Ed.), Materials science of the earth's interior, pp. 303-330.

Sverjensky, D.A., Stagno, V., Huang, F., 2014. Important role for organic carbon in subduction-zone fluids in the deep carbon cycle. Nature Geoscience 7, 909-913.

Syracuse, E.M., van Keken, P.E., Abers, G.A., 2010. The global range of subduction zone thermal models. Physics of the Earth and Planetary Interiors 183, 73-90.

Tappert, R., Stachel, T., Harris, J.W., Muehlenbachs, K., Ludwig, T., Brey, G.P., 2005. Subducting oceanic crust: The source of deep diamonds. Geology 33, 565-568.

Tassinari, C.C.G., Teixeira, W., Siga, J.O., 1989. Archaean and early Proterozoic crustal evolution of Amazonian craton, Brazil. 28th International Geological Congress, 22.

Taylor, W.R., Canil, D., Milledge, H.J., 1996. Kinetics of Ib to IAa nitrogen aggregation in diamond. Geochimica Et Cosmochimica Acta 60, 4725-4733.

Taylor, W.R., Jaques, A.L., Ridd, M., 1990. Nitrogen-defect aggregation characteristics of some australasian diamonds - time-temperature constraints on the source regions of pipe and alluvial diamonds. American Mineralogist 75, 1290-1310.

Thomazo, C., Ader, M., Philippot, P., 2011. Extreme ^{15}N-enrichments in 2.72-gyr-old sediments: Evidence for a turning point in the nitrogen cycle. Geobiology 9, 107-120.

Thomazo, C., Pinti, D.L., Busigny, V., Ader, M., Hashizume, K., Philippot, P., 2009. Biological activity and the earth's surface evolution: Insights from carbon, sulfur, nitrogen and iron stable isotopes in the rock record. Comptes Rendus Palevol 8, 665-678.

Thomson, A.R., Kohn, S.C., Bulanova, G.P., Smith, C.B., Araujo, D., Walter, M.J., Eimf, 2014. Origin of sub-lithospheric diamonds from the Juina-5 kimberlite (Brazil): Constraints from carbon isotopes and inclusion compositions. Contributions to Mineralogy and Petrology 168.

Toth, J.R., 1980. Deposition of submarine crusts rich in manganese and iron. Geological Society of America Bulletin 91, 44-54.

Tribuzio, R., Messiga, B., Vannucci, R., Bottazzi, P., 1996. Rare earth element redistribution during high-pressure-low-temperature metamorphism in ophiolitic Fe-gabbros (Liguria, northwestern Italy): Implications for light REE mobility in subduction zones. Geology 24, 711-714.

Usui, A., Someya, M., 1997. Distribution and composition of marine hydrogenetic and hydrothermal manganese deposits in the northwest Pacific, Manganese mineralization: Geochemistry and Mineralogy of Terrestrial and Marine Deposits, pp. 177-198.

van Heerden, L.A., 1993. A nitrogen and carbon stable isotope study of some Western Australian diamonds, Department of Earth Sciences. The Open University, Milton Keynes.

van Heerden, L.A., Boyd, S., H.J., M., Pillinger, C.T., 1995. The carbon- and nitrogen-isotope characteristics of the Argyle and Ellendale diamonds, Western Australia. International Geology Review 37, 39-50.

Walter, M.J., 1998. Melting of garnet peridotite and the origin of komatiite and depleted lithosphere. Journal of Petrology 39, 29-60.

Walter, M.J., Bulanova, G.P., Armstrong, L.S., Keshav, S., Blundy, J.D., Gudfinnsson, G., Lord, O.T., Lennie, A.R., Clark, S.M., Smith, C.B., Gobbo, L., 2008. Primary carbonatite melt from deeply subducted oceanic crust. Nature 454, 622-U630.

Walter, M.J., Kohn, S.C., Araujo, D., Bulanova, G.P., Smith, C.B., Gaillou, E., Wang, J., Steele, A., Shirey, S.B., 2011. Deep mantle cycling of oceanic crust: Evidence from diamonds and their mineral inclusions. Science 334, 54-57.

Wentorf, R.H., 1970. Some studies of diamond growth rates - phys. Abstracts of Papers of the American Chemical Society, 69-&.

Wilson, C.R., Spiegelman, M., van Keken, P.E., Hacker, B.R., 2014. Fluid flow in subduction zones: The role of solid rheology and compaction pressure. Earth and Planetary Science Letters 401, 261-274.

Woods, G.S., Collins, A.T., 1983. Infrared-absorption spectra of hydrogen complexes in type-I diamonds. Journal of Physics and Chemistry of Solids 44, 471-475.

Wyman, D.A., Ayer, J.A., Conceicao, R.V., Sage, R.P., 2006. Mantle processes in an Archean orogen: Evidence from 2.67 ga diamond-bearing lamprophyres and xenoliths. Lithos 89, 300-328.

Wyman, D.A., O'Neill, C., Ayer, J.A., 2008. Evidence for modern-style subduction to 3.1 Ga: A plateau-adakite-gold (diamond) association, in: Condie, K.C., Pease, V. (Eds.), When did plate tectonics begin on planet earth, pp. 129-148.

Figure Captions

Figure 1. Primitive mantle-normalised trace element pattern for the Dachine ultramafic host rock compared to averages for kimberlite (Group I), komatiite and boninite (global averages from the Georoc database: http://georoc.mpch-mainz.gwdg.de/georoc/Start.asp) and the Wawa diamondiferous lamprophyre (Wyman et al., 2006). The inset shows Th/Nb (high ratio is indicative of wedge mantle source) vs Gd/Yb (high ratio indicative of garnet-bearing residue) with data sources as in the main figure, and with the inclusion of average shoshonite and island arc calc-alkaline basalt.

Figure 2. Cathodoluminescence images of four Dachine diamonds showing representative internal structures. a) Irregular octahedral aggregate external form. Internally it displays polycentric cubo-octahedral blocky sectorial growth centres, in part showing vermiform granular texture due to dislocations and intense plastic deformation; b) irregular octahedral diamond with blocky polycentric internal structure and prominent etch channels; c) cubo-octahedron with weak internal zonation. Rim shows fibrous growth; one separate block in bottom right is apparent; d) cubo-octahedron with cuboid zoning and intensive plastic deformation.

Figure 3. FTIR spectra of type Ib diamonds containing i) 255 ii) 103 and iii) 48 ppm N as a mix of C- and A-centres". Panels iv) and v) show type IIa diamonds with features similar to the F-defect (Woods and Collins, 1983).

Figure 4. $\delta^{15}N$ v $\delta^{13}C$ plot of isotopic compositions of Dachine diamonds compared to other global sources of mantle diamond. Dachine data from this study are shown as solid circles and the data from Cartigny (2010) are shown as open triangles. Error bars shown for the $\delta^{15}N$ values take into account the uncertainties after the blank correction. The comparative fields are sourced from the following references: eclogitic diamonds (Cartigny et al., 1998, 1999; van Heerden, 1993; van Heerden et al., 1995; Bulanova et al.,1999, 2002); diamondites and carbonado (Gautheron et al.,

2005; Mikhail et al., 2013; Shelkov et al., 1997); peridotitic diamonds (Cartigny et al., 1997, 1999; 2004); and crustal organic carbon (Thomazo et al., 2009, 2011).

Figure 5. Garnet compositions from Dachine diamond inclusions compared with crustal and mantle-derived garnet from Dachine host rock crustal concentrates (Bailey, 1999), and with sulfide-associated garnet from Broken Hill (New South Wales) (Spry and Wonder, 1989) and Balfour (Tasmania) (Bottrill, 2004), VMS sulphide deposits from Abitibi (Canada) (Dubé et al., 2007) and Pecos (New Mexico) (Slack et al., 2009), and Mn-rich gondite deposits from Ghana (Melcher, 1995). Inset photo shows a backscattered electron image of the garnet inclusion in diamond DACBS 4A-11. The inset figure shows CaO vs Cr_2O_3 and illustrates the eclogitic nature of the garnet inclusions; fields E-eclogitic, L-lherzolitic, H-harzburgitic, W-wehrlitic after (Aulbach et al., 2002).

Figure 6. Compatibility diagram showing primitive mantle normalized (McDonough and Sun, 1995) trace element contents of Dachine garnet inclusions. The inset shows La_N versus Yb_N for the Dachine garnet inclusions compared to garnet inclusions in lithospheric and sublithospheric diamonds and diamondite (E-type=eclogitic; P-type=peridotitic) (Bulanova et al., 2010; Dobosi and Kurat, 2010; Stachel et al., 2004; Thomson et al., 2014).

Figure 7. Dachine clinopyroxene inclusions and host rock concentrate clinopyroxenes (drill core) plotted on a pyroxene ternary diagram. Fields show peridotitic (P-type) and eclogitic (E-type) clinopyroxene inclusions in lithospheric diamonds (Bulanova, 1995; Meyer, 1987; Morris et al., 2002). The inset is a back scattered SEM image of the clinopyroxene inclusion in Dachine diamond DACBS 4B-07.

Figure 8. Compatibility diagram showing primitive mantle normalized (McDonough and Sun, 1995) trace element contents of Dachine clinopyroxene inclusions (Table 3). Inset shows La_N versus $(Gd/Lu)_N$ for Dachine clinopyroxene inclusions relative to eclogitic and peridotitic

clinopyroxene inclusions in lithospheric diamonds, as well as clinopyroxenes in diamondite (Bulanova et al., 2010; Dobosi and Kurat, 2010; Stachel et al., 2004).

Figure 9. Pressure-temperature plot showing thermobarometric results for xenocrystic Cr-diopside from the Dachine host rock drill core concentrates using the thermobarometer of Nimis and Taylor (2000). Also shown is a conductive geotherms 45 mW/m^2 (after Pollack and Chapman, 1977), the position of the graphite to diamond phase boundary (after Bundy, 1989), and the pressure for the majoritic garnet inclusion obtained in this study.

Figure 10. Dachine sulfide inclusions plotted in the Fe-S-Ni system. Tie lines connect the compositions of phases in unmixed inclusions. The inset photos show backscattered electron images of representative Dachine inclusion. The inset figure shows Ni vs Cr for Dachine inclusions (only single phase inclusions shown) compared to examples of inclusions from lithospheric diamonds of either peridotitic or eclogitic affinity (Stachel and Harris, 2008).

Figure 11. (a) N vs %1aA aggregation in Dachine diamonds. Data from this study are shown as solid circles, and those from Cartigny (2010) are shown as open circles. The curve is the best fit to the data assuming a single temperature-time history for all diamonds, which we call a thermal isopath. (b) Temperature (°C) – time curves for diamond with 200 ppm N and 45% C to A aggregation (i.e. 45% 1aA). The curves are calculated using experimentally determined values for C to A kinetics of lnA = 18.8 and Ea = 6.0 eV in natural cubic sector diamond (Taylor et al., 1996).

Figure 12. Primitive mantle normalized abundances of rare earth elements (REE) (McDonough and Sun, 1995), with Dachine garnet (a) and clinopyroxene (b) shown in grey. Modeled REE abundances are shown for comparison, assuming initial source abundances of average normal MORB from the East Pacific ridge (Klein, 2003). Partitioning coefficients between garnet, clinopyroxene and liquid are from (Kessel et al., 2005a) at 6 GPa and 800 °C, and between allanite and melt from (Klimm et al., 2008) at 2.5 GPa, 800 °C. A model for a simple garnet +

clinopyroxene lithology (0.5:0.5 in mode) is shown as a light blue line. A model for 20% melt depletion, assuming modal melting and 20% batch melt extraction is shown as a red line. A model with a garnet:cpx:allanite mineral mode of 0.495:0.495:0.01 is shown as a purple line. A model starting with a source having elemental abundances composed of 90% average normal MORB + 10% world ocean average ferromanganese crust (AV-1 in Baturin et al. (2012), and a garnet/cpx/allanite mineral mode of 0.495/0.495/0.01 is shown as a dark blue line.

Figure 13. Primitive mantle normalized abundances of non-REE transition metal elements (McDonough and Sun, 1995), with average Dachine garnet (a) and clinopyroxene (b) shown in grey. Models for REE abundances are shown for comparison with original elemental abundances of average normal MORB from the East Pacific ridge (Klein, 2003). Partition coefficients between garnet, clinopyroxene and liquid are from (Kessel et al., 2005a; Pertermann et al., 2004). For rutile they are from (Klemme et al., 2005). A model for a simple garnet + clinopyroxene lithology (0.5:0.5) is shown as a light blue line. A model starting with elemental abundances of 80% average normal MORB + 20% world ocean average ferromanganese crust (AV-1 in Baturin et al. (2012), and a garnet/cpx mineral mode of 0.5/0.5 is shown as a dark blue line. The purple line shows the same model but with the addition of 5% rutile added to the mode proportionally.

Figure 1

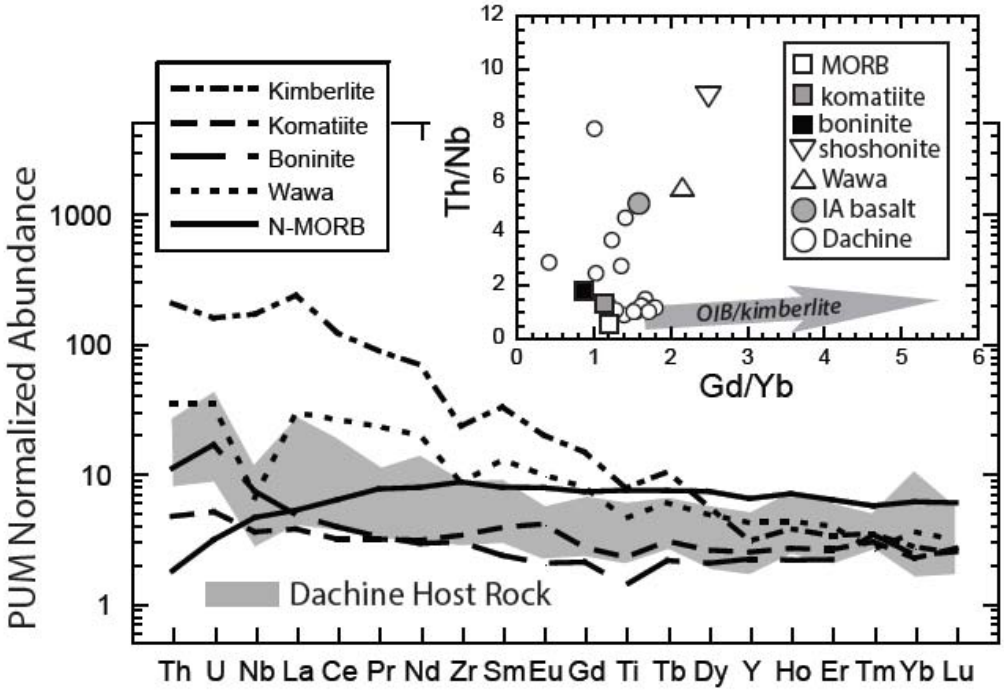

Figure 2

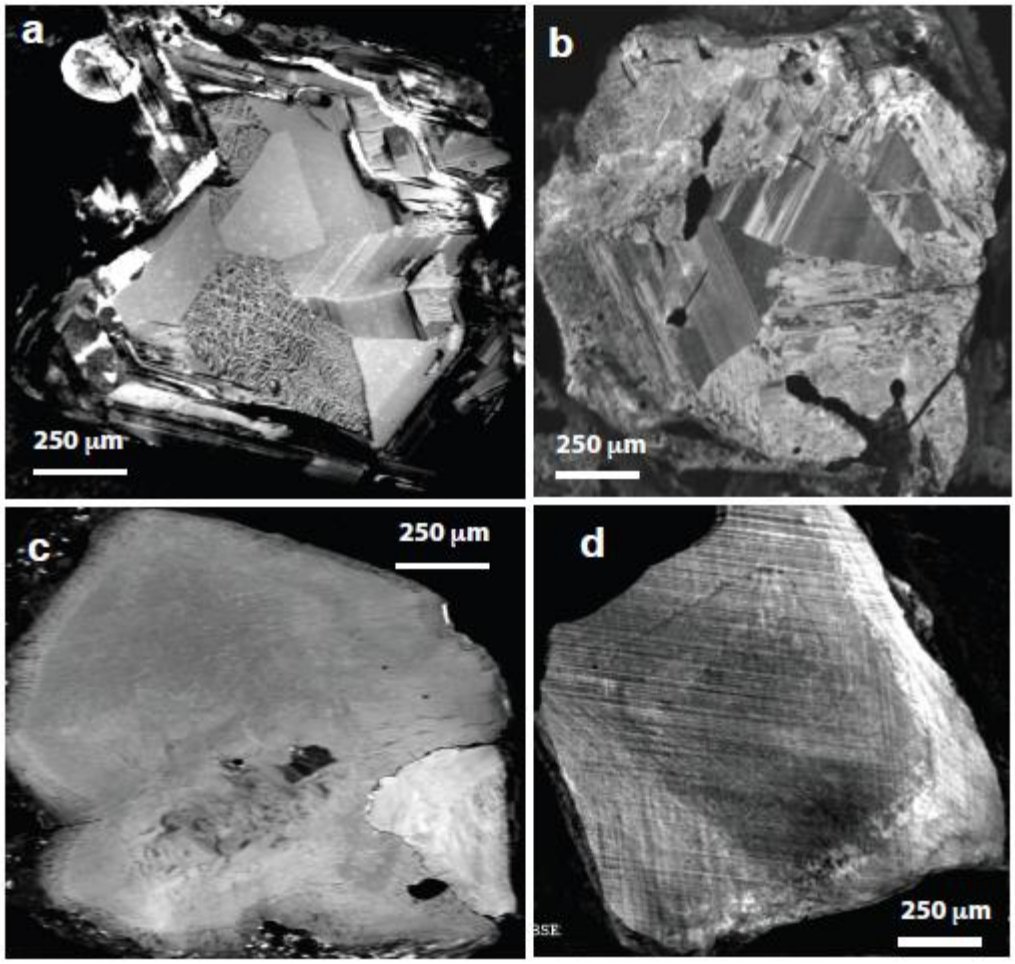

Figure 3

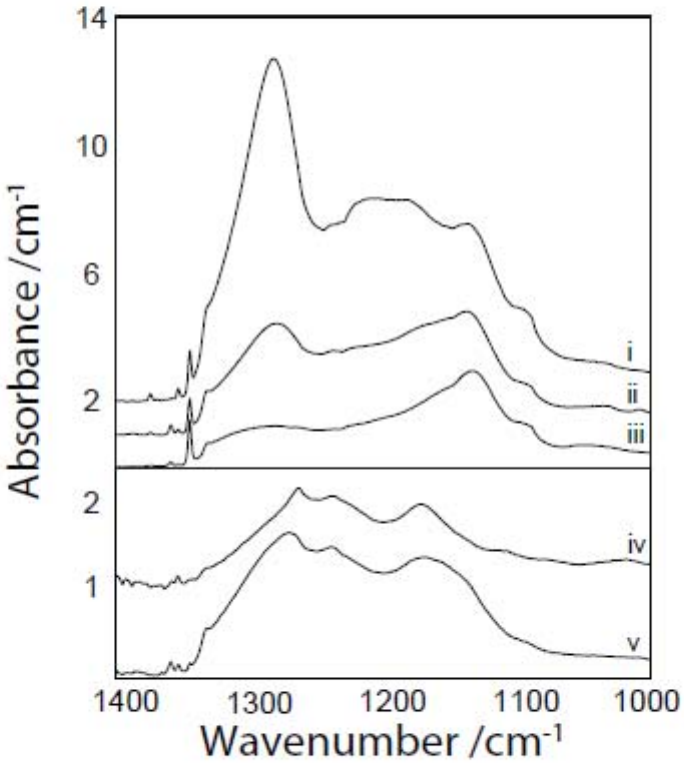

Figure 4

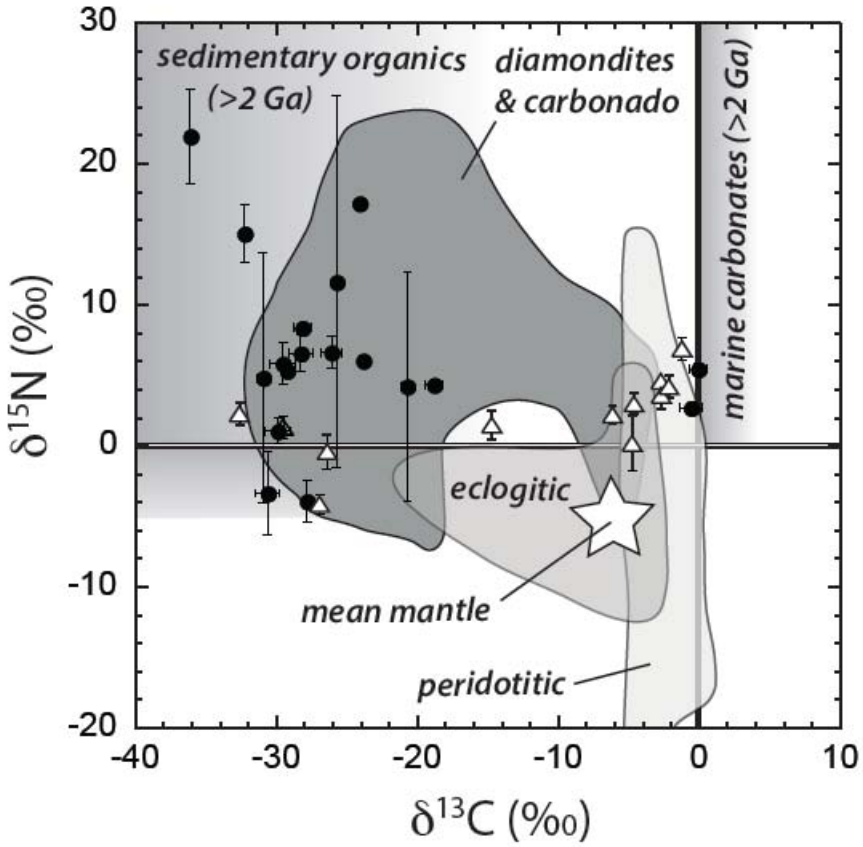

Figure 5

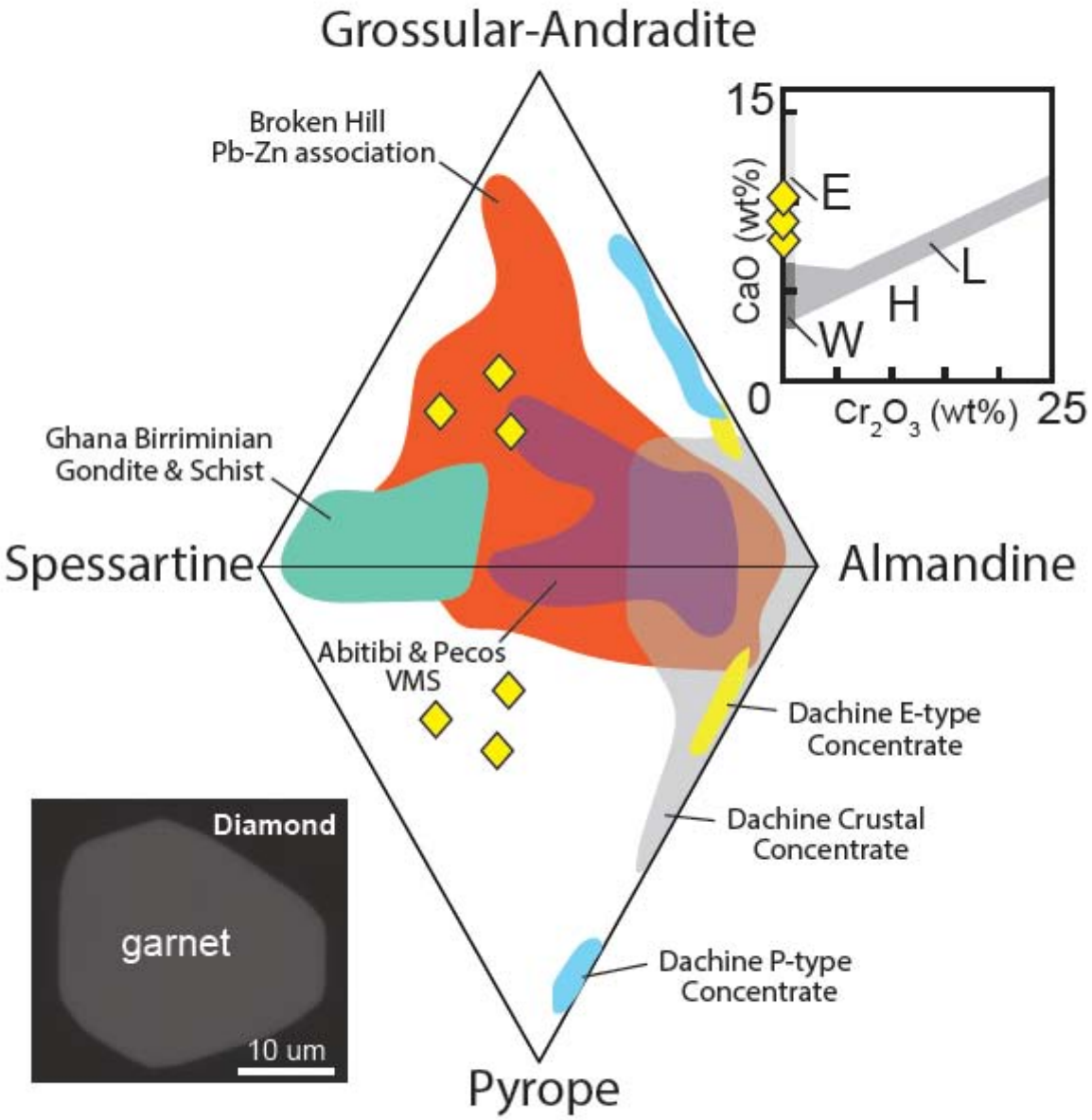

Figure 6

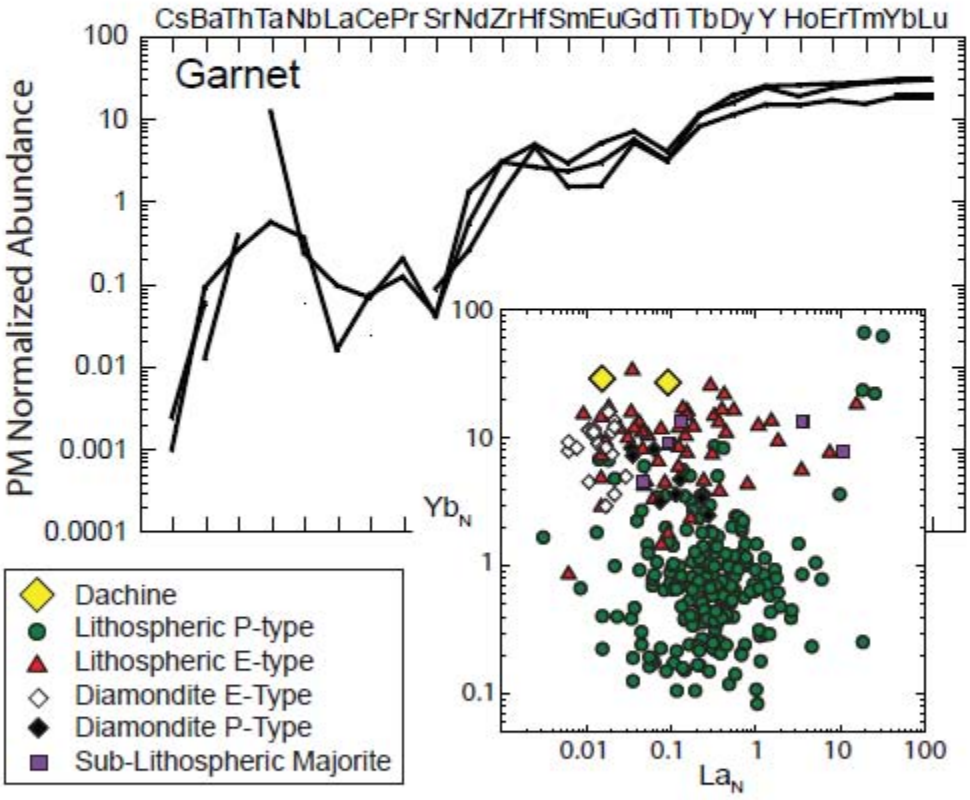

Figure 7

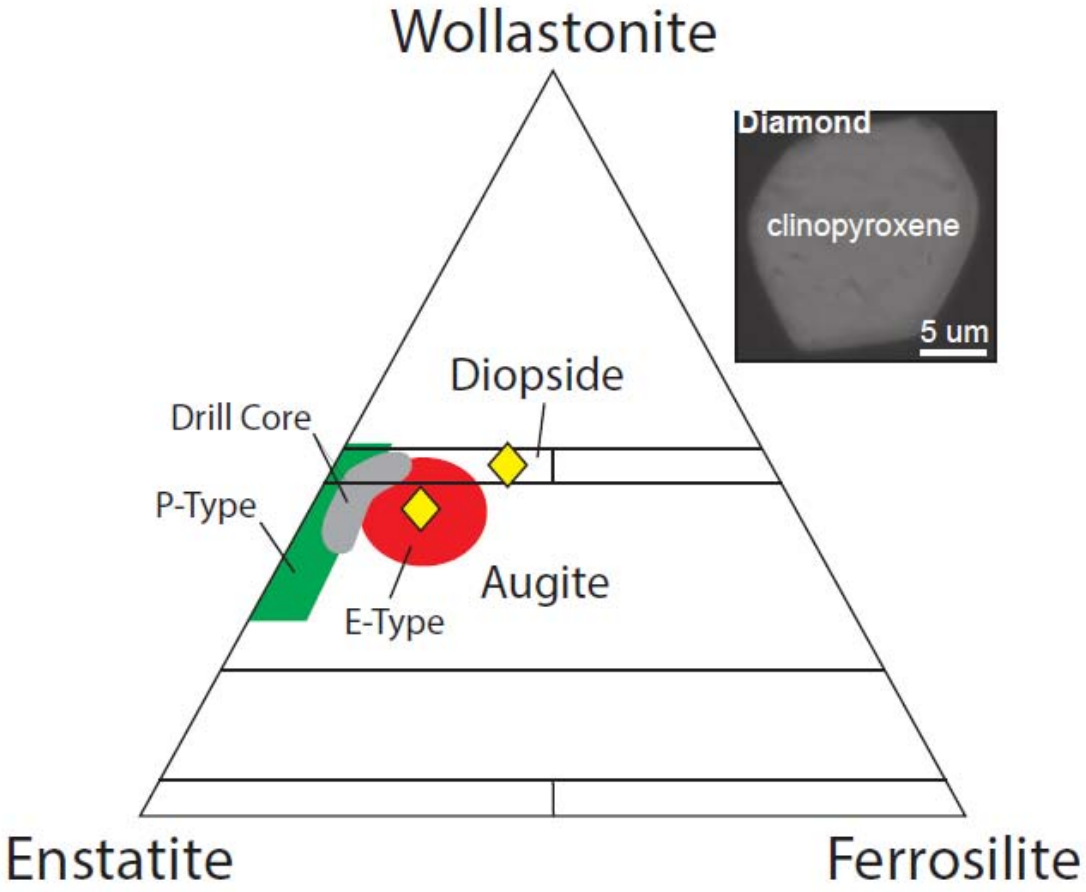

Figure 8

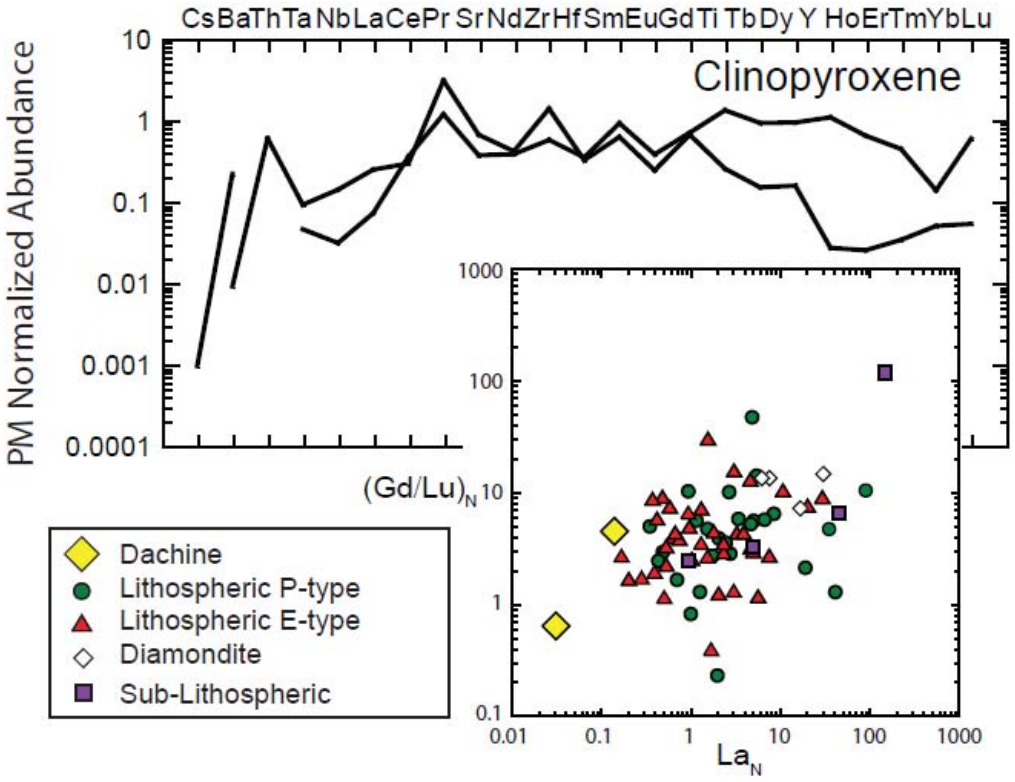

Figure 9

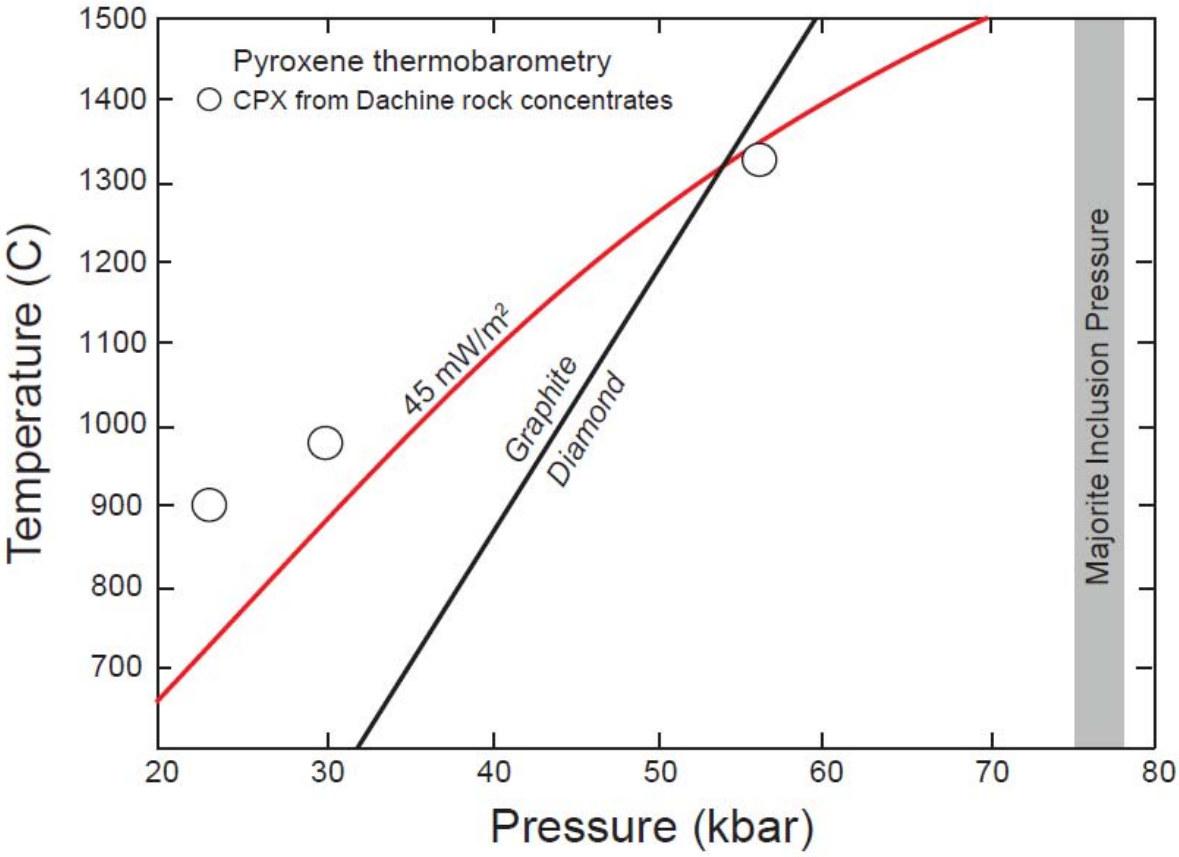

Figure 10

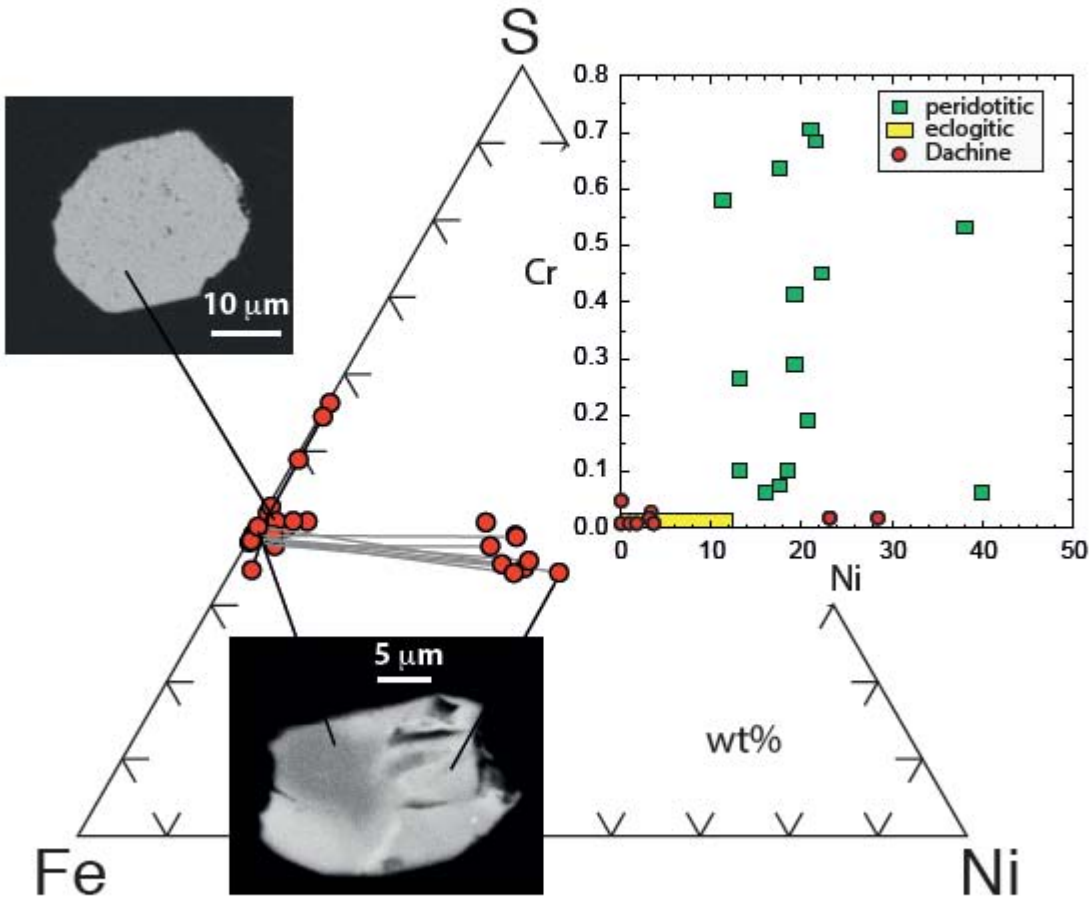

Figure 11

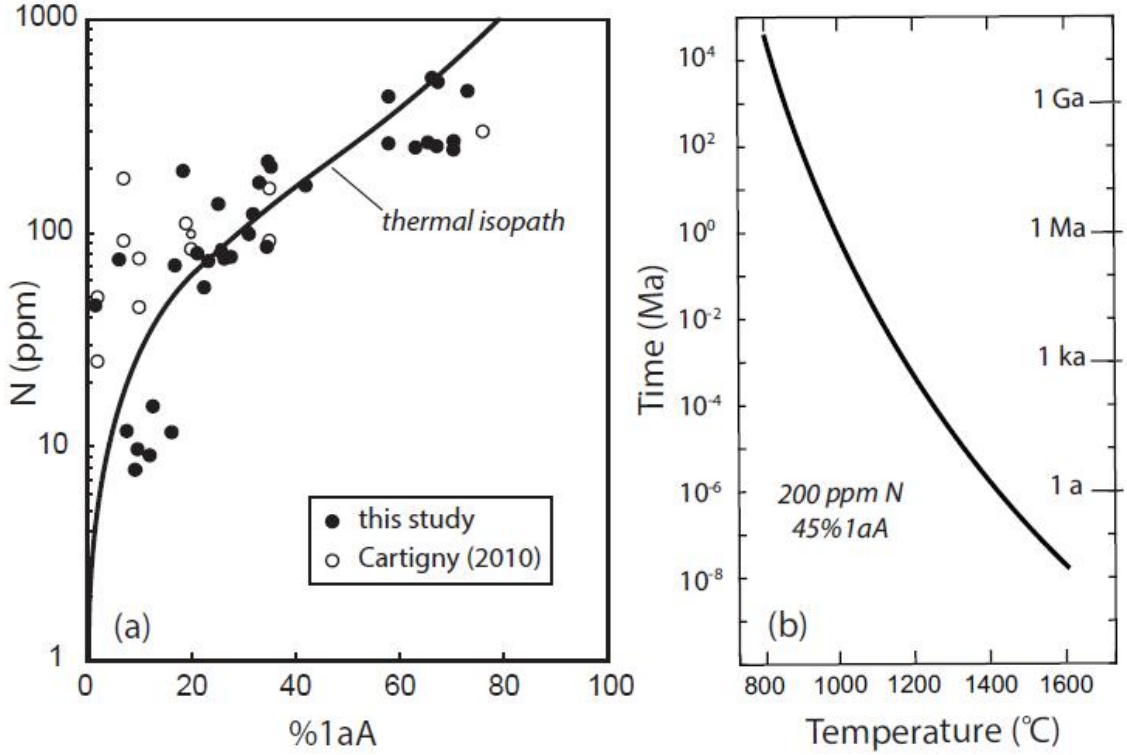

Figure 12

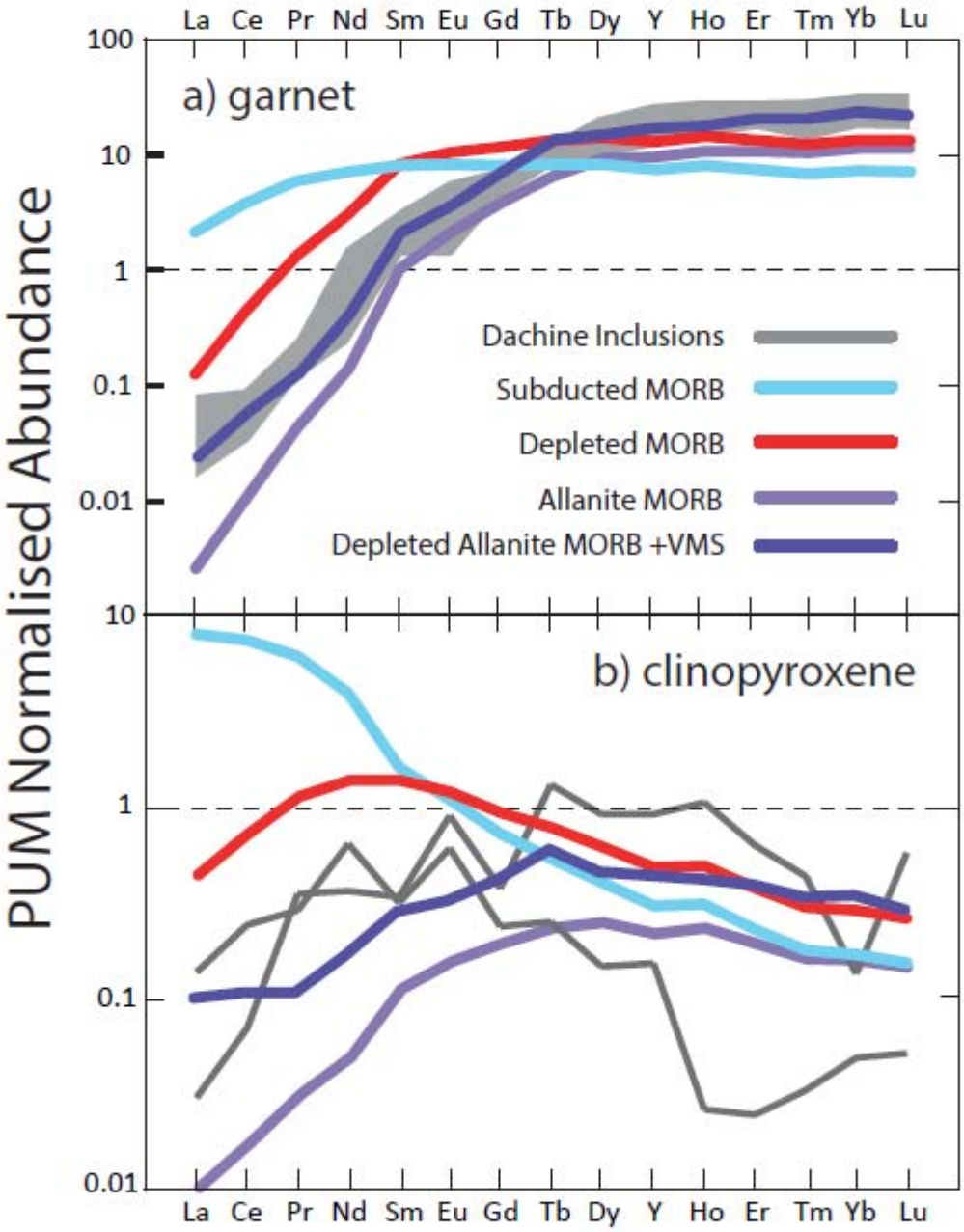

Figure 13

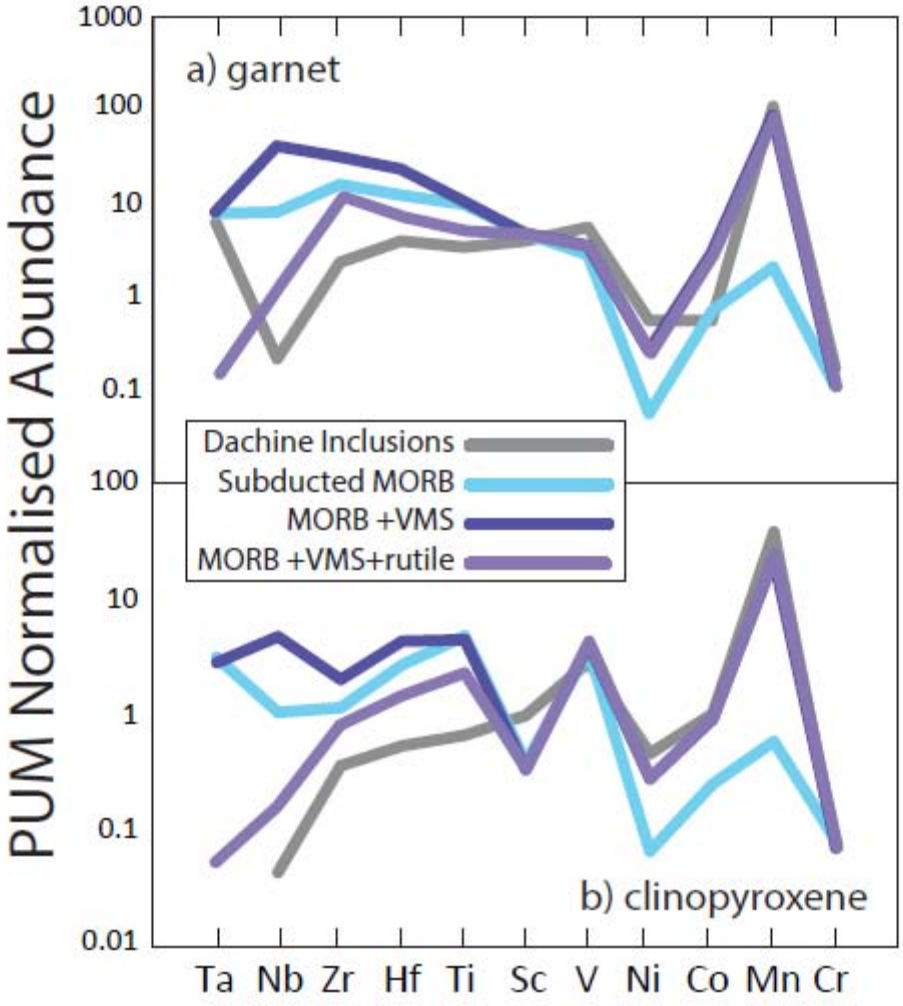

Table 1. Carbon and Nitrogen abundances and isotopic compositions of Dachine Diamonds

Sample	C (mg)[a]	N ppm	$\delta^{13}C$[b]	±	$\delta^{15}N$[c]	±
JR-405-5	0.123	5	-20.67	0.49	4.19	10.88
DAC101 Y	0.73	39	0.08	0.51	4.1	1.0
DAC101 W	0.8	26	-0.6	0.8	2.46	0.45
DAC102	0.625	9	-26.07	0.7	7.1	1.0
DAC103	0.561	8	-30.11	0.89	0.0	2.8
DAC104	0.693	19	-18.78	0.62	5.06	0.57
DAC105	0.745	8	-28.23	0.82	8.59	1.47
DAC45-2	0.94	5	-29.52	0.88	5.66	2.26
DAC45-3	0.6	53	-28.12	0.58	8.33	0.34
DAC45-6	0.685	34	-29.21	0.38	8.79	2.94
DAC45-9	0.758	110	-24.06	0.21	17.15	0.33
DAC45-4	0.621	3	-30.90	0.43	-	-
DAC45-7	0.51	9	-36.07	0.19	19.01	2.23
BS-4A-12	0.317	-	-25.93	0.15	-	-
JR-A01-4	0.531	2	-25.70	0.32	-	-
DAC45-8	0.826	11	-32.23	0.21	4.23	0.94
DAC106	0.585	3	-30.66	0.29	-	-
DAC107	0.549	3	-27.81	0.22	-3.94	2.54
BS-4B-N3	0.31	16	-23.81	0.18	5.7	1.4

a - total weight of diamond analysed

b - $\delta^{13}C = [(^{13}C/^{12}C)_{sample}/(^{13}C/^{12}C)_{standard} - 1] \times 1000$

c - $\delta^{15}N = [(^{15}N/^{14}N)_{sample}/(^{15}N/^{14}N)_{standard} - 1] \times 1000$

Table 2. Major and minor element compositions of silicate inclusions (wt.%)

Diamond	4A-5	4A-11	4B-2	4A-2	4B-7
Mineral	Garnet			Clinopyroxene	
SiO_2	37.6	38.5	39.9	54.7	52.1
TiO_2	0.62	0.85	0.6	0.14	0.15
Al_2O_3	20.1	20.4	20.5	6.72	0.98
Cr_2O_3	0.05	0.06	0.08	0.14	0
FeO	12.5	6.68	8.01	9.44	7.78
MnO	15.1	18.8	12.8	0.09	4.6
MgO	4.99	5.98	6.9	8.62	14.6
CaO	7.67	8.64	10.2	16.9	17.9
Na_2O	0.03	0.03	0.12	3.43	0.44
K_2O	-	-	-	0.02	0.21
ZnO	0.01	0.06	-	-	0.22
Total	98.7	100.0	99.1	100.2	99.0
Si	3.00	3.00	3.07	2.00	1.98
Ti	0.04	0.05	0.03	0.00	0.00
Al	1.89	1.87	1.86	0.29	0.04
Cr	0.00	0.00	0.00	0.00	0.00
Fe	0.83	0.43	0.52	0.29	0.25
Mn	1.02	1.24	0.83	0.00	0.15
Mg	0.59	0.69	0.79	0.47	0.82
Ca	0.65	0.72	0.84	0.66	0.73
Na	0.00	0.00	0.02	0.24	0.03
K	0.00	0.00	0.00	0.00	0.01
Zn	0.00	0.01	0.00	0.00	0.01
cations	8.03	8.02	7.97	3.97	4.02

oxygens	12.0	12.0	12.0	6.00	6.00
almandine	26.9	14.1	17.3	-	-
pyrope	19.1	22.5	26.6	-	-
grossular	21.1	23.3	28.1	-	-
spessartine	32.9	40.1	28.0	-	-
wollastonite	-	-	-	46.6	40.4
enstatite	-	-	-	33.1	45.9
ferrosilite	-	-	-	20.3	13.7
P (GPa)[a]	-	-	7.7	-	-
T (^{o}C)[b] 4A-2	1726	2376	2595	-	-
T (^{o}C) 4B-7	1296	1722	1988	-	-

a - P = pressure in GPa using the garnet barometer of Collerson (2010)

b - T = temperaure in ^{o}C using the garnet-cpx thermometer of Nakamura (2009)

Table 3. SIMS trace element analyses of silicate inclusions (ppm)

Diamond	D-BS4A-5 gt	D-BS4A-11 gt	D-BS4B-2 gt	D-BS4B-7cpx	D-BS4A-2 cpx
Mineral	garnet	garnet	garnet	clinopyroxene	clinopyroxene
Rb	<3	<3	<1.5	<1	<1
Cs	nd	0.05	0.02	0.02	nd
Ba	0.08	0.38	0.58	1.4	0.06
Th	0.03	nd	0.02	nd	nd
U	nd	0.02	nd	nd	nd
Nb	0.05	0.15	0.23	0.03	0.06
Ta	nd	0.44	0.02	nd	0.02
La	nd	0.06	0.01	0.02	0.09
Ce	0.04	0.11	0.12	0.12	0.41
Pr	nd	0.05	0.03	0.09	0.07
Sr	1.69	0.78	0.82	23.3	60.9
Nd	0.31	1.56	0.67	0.46	0.82
Zr	12.7	30.6	30.2	3.95	4.35
Hf	1.25	1.34	0.73	0.16	0.39
Sm	0.59	1.14	0.91	0.15	0.13
Eu	0.23	0.75	0.44	0.14	0.10
Gd	2.72	3.80	3.10	0.21	0.13
Tb	0.78	1.09	1.06	0.13	0.03
Dy	7.25	10.20	12.50	0.62	0.10
Y	61.4	98.8	104.1	3.99	0.67
Ho	2.10	2.70	3.69	0.16	0.004
Er	7.10	9.96	11.3	0.28	0.01
Tm	0.99	1.77	1.81	0.03	0.002
Yb	7.90	12.10	12.87	0.06	0.02
Lu	1.22	1.97	2.01	0.04	0.004

Sc	57.0	68.3	65.2	16.4	28.3
Li	1.99	2.89	3.20	12.94	22.25
P	84.0	9.72	10.77	4.18	4.51
V	448.0	533.8	352.8	242.0	226.7
Cr	431.6	421.1	458.1	194.09	0.16
Ni	1493	775.6	956.7	926.8	102.4
Co	85.2	46.1	44.5	110.0	133.4
Ga	79.2	87.1	77.2	31.4	11.7
Mo	<0.07	<0.14	<0.06	<0.05	0.17
Sn	4.59	16.05	4.48	4.48	0.66
Cu	nd	nd	nd	nd	26.7
Zn	nd	nd	nd	nd	80.5

nd - not detected

Table 4. Electron microprobe analyses of syngenetic sulphide inclusions from Dachine diamonds (wt%)

Diamond	Incl. No	Mineral	Fe	Ni	Co	Cu	S	Zn	Cr	Mn	Total
DAC 45-1	1	Po[a]	57.4	3.36	0.24	0.52	40.7	0.03	0.03	0.02	102.4
DAC 45-2	1	Po	56.9	0.58	0.06	0.79	40.0	-	-	-	98.3
DAC 45-3	1	Po	56.0	0.6	0.09	1.44	39.1	-	-	-	97.2
DACBS 4A -1	1	Po	57.8	0.31	0	0.19	38.4	0.01	0.01	-	96.7
DACBS 4A -1	2	Po	57.9	0.31	0	0.21	42.0	0.04	0	0.02	100.5
DACBS 4A-2	1-1 core	Pn[b]	27.4	35.1	1.56	0.65	32.5	-	-	-	97.3
DACBS 4A-2	1-2 rim	Po	56.8	0.54	0.09	0.69	38.5	-	-	-	96.6
DACBS 4A-2	2-1core	Cu-Fe	25.6	0.13	0.04	43.0	30.8	-	-	-	99.4
DACBS 4A-2	2-2rim	Po	55.2	0.49	0.08	4.53	37.0	-	-	-	97.3
DACBS 4A -4	1-1	Pn	30.1	28.4	1.56	0.38	37.5	-	0.02	-	98.0
DACBS 4A -4	1-2	Po	59.1	1.07	0	0.17	41.7	0.04	0	0.02	102.0
DACBS 4A-4	2-1 core	Po	59.7	0.15	0.11	0.17	37.9	-	-	-	98.0
DACBS 4A-4	2-2 rim	Pn	33.1	28.5	1.65	0.14	33.6	-	-	-	96.9
DACBS 4A-4	3-1	Pn	32.0	30.0	1.76	0.33	32.2	-	-	-	96.3
DACBS 4A-6	1-1core	Po	59.7	0.18	0.05	0.46	37.9	-	-	-	98.3
DACBS 4A-6	1-2 rim	Pn	29.4	30.6	4.28	0.78	33.4	-	-	-	98.6

DACBS 4A-6	2-1	Po	53.7	0.18	0.07	6.17	36.0	-	-	-	96.1
DACBS 4A-6	3-1	Po	58.1	0.1	0.08	2.27	37.7	-	-	-	98.2
DACBS 4A-7	1	Po	56.8	0.33	0.01	3.88	38.1	-	-	-	99.0
DACBS 4A-8	1-1 hom.	Po	52.8	0.2	0.13	2.98	34.8	-	-	-	90.9
DACBS 4A-8	1-1 rep.	Po	58.9	0.14	0	1.11	37.9	-	-	-	98.1
DACBS 4A-8	2	Po	59.0	0.17	0	0.99	37.9	-	-	-	98.1
DACBS 4A-8	3	Po	58.8	0.16	0	0.8	38.4	-	-	-	98.2
DACBS 4A-9	1	Po	59.5	0.19	0	0.06	39.0	-	-	-	98.8
DACBS 4A -12	1	Po	58.6	0.24	0.03	0.35	44.1	0.03	0.01	0.05	103.4
DACBS 4A-12	1	Po	57.7	0.33	0	0.96	38.6	-	-	-	97.5
DACBS 4A-12	2	Po	58.2	0.37	0.06	0.21	39.5	-	-	-	98.3
DACBS 4B-1	1	Po	61.4	0.05	0	0.4	40.0	0.01	0.01	0.01	101.9
DACBS 4B-10	1	Po	59.5	0.2	0	0.66	37.2	-	-	-	97.5
DACBS 4B-4	1	Po	58.2	0.21	0.11	0.36	39.2	-	-	-	98.1
DACBS 4B-5	1	Po	54.8	2.31	0.09	0.68	36.3	-	-	-	94.2
DACBS 4B-5	1-rim	Pn	33.4	26.3	1.75	0.44	36.0	-	-	-	97.8
DACBS 4B-5	1 core	Po	57.7	3.15	0.02	0.62	36.8	-	0.02	0.01	98.4
DACBS 4B-5	2 rim	Po	58.8	0.99	0	0.48	40.1	0.01	0.01	0.01	100.4

DACBS 4B-6	1-1 core	Po	57.1	1.04	0.07	1.29	37.3	-	-	-	96.8
DACBS 4B-6	1-2 rim	Pn	26.0	24.7	2.56	11.8	32.3	-	-	-	97.3
DACBS 4B-9	1	Po	57.8	0.04	0.01	0.38	37.4	-	-	-	95.7
JR A01-1	1	Po	55.3	2.24	0.16	3.9	37.0	-	-	-	98.6
JR A01-2	1-1	Po	51.6	0.27	0.46	0.05	49.7	-	-	-	102.1
JR A01-2	1-2	Chp[c]	27.7	0.09	0.05	30.7	35.7	-	-	-	94.2
JR A01-3	1-1	Po	59.7	0.08	0	0.59	38.0	-	-	-	98.3
JR A01-3	1-2	Pn	30.7	23.1	2.17	4.71	37.0	-	0.02	0.02	97.7
JR A01-3	2	Po	59.9	0.06	0	0.96	40.3	0.03	0.05	0.01	101.3
JR A01-3	3	Po	54.9	3.64	0.21	0.93	40.5	0.01	0.01	-	100.3

a - Pyrrhotite; b - Pentlandite; c - Chalcopyrite

Diamonds from Dachine, French Guiana: a unique record of Early Proterozoic subduction

Chris B. Smith, Michael J. Walter, Galina P. Bulanova, Sami Mikhail, Antony D. Burnham, Luiz Gobbo, and Simon C. Kohn

Highlights

- Dachine diamonds have C and N isotopic compositions indicating a sedimentary source
- Disaggregated nitrogen defects severely limit diamond residence time in the mantle
- Garnet and clinopyroxene inclusions are eclogitic and indicate a metal-rich source
- Inclusion and xenocryst thermobarometry indicates formation at ~200 - 250 km depth
- We suggest a model for diamond growth at the slab mantle interface in a subduction zone